Analysis of an Embedded Singularity based Chipless RFID Tag

Andrew Travis Blischak

Thesis submitted to the faculty of the
Virginia Polytechnic Institute and State University
in partial fulfillment of the requirements for the degree of

Master of Science
in
Electrical and Computer Engineering

Majid Manteghi, Chair
William A. Davis
Ahmad Safaai-Jazi

June 30th, 2011
Blacksburg, Virginia

Keywords: Chipless, RFID, SEM, Pole, Matrix Pencil

Analysis of an Embedded Singularity based Chipless RFID Tag

Andrew Travis Blischak

ABSTRACT

The objective of this research is to explore the feasibility of a chipless RFID tag that stores a data signature in the form of complex frequency plane singularities. To this end an existing chipless RFID tag, the notched elliptical dipole tag, was analyzed first with simulations and then measurements. A pole signature was extracted from simulations, and individual poles were determined via experimentation to be attributable to specific controllable features of the tag. The poles were shown to be independent of both excitation and observation. A prototype tag was measured, and the pole signature was retrieved from the scattered fields. The tag was successfully read for different orientations showing that embedded singularities can be used as a means for encoding and retrieving data.

ACKNOWLEDGEMENTS

I would like to thank my advisor, Dr. Manteghi, for the patience he displayed, which was much more than I deserved. I thank Dr. Davis and Dr. Safaai-Jazi for serving on my committee. For their assistance formulating and taking measurements, I thank Randall Nealy, Taeyoung Yang, and Dr. Davis. Lastly, I thank my family not for what I would call encouragement, but rather prodding.

All photos by author, 2011

Table of Contents

LIST OF FIGURES

Chapter 2: Singularity Expansion Method (SEM)

LIST OF TABLES

Chapter 2: Singularity Expansion Method (SEM)

Chapter 3: Notched Elliptical Dipole Tag

CHAPTER 1

Introduction

The basic concept of an RFID tag has been around since the early part of the 20th century [1]. The modern incarnation of the passive RFID tag relying on modulation of back scattered signals was first proposed and demonstrated in the 70s, and is currently the most prevalent form of RFID tag. RFID tags are versatile and can be attached to or incorporated into a wide range of objects. Typically these tags consist of a silicon chip to modulate the backscattered signal and an antenna to both receive the energy necessary to power the chip and transmit the backscattered signal [2]. As a generality, RFID tags fall into one of two categories: active tags requiring an internal power source, and passive tags which rely on an external power source. The most common form of passive RFID tags are powered by electrical currents induced in an integral antenna which powers an integrated circuit, the ASIC. The IC then transmits its signal via modulation of a backscattered signal to the reader. In their current form, passive tags are usually readable from a distance ranging from 10cm up to several meters, using frequencies in the 13.56 MHz (HF) or the UHF ISM band from (902 to 928 MHz). The absence of an internal power source allows these tags to be compact and have a very long life span.

This thesis considers a new class of passive RFID tags which eliminates the need for a chip, and does not require any auxiliary components such as antennas or transmission lines. A “chipless” RFID is not a new concept in itself, as several concepts

have been presented [3-10]. A surface acoustic wave (SAW) device has been used as a wireless passive sensor. SAW devices rely on a time-gating technique to separate the sensed data from environmental reflections. SAW based tags are inherently costly, making them more expensive than silicon based tags. The SAW wireless sensor tag based on mismatch techniques inspired another group to design a chipless RFID using a transmission-line network to create mismatches and thus store information [11]. Using a mismatch based approach has a fundamental difficulty due to the ambiguity between multiple reflections inside the device and reflections due to the environment. Transmission lines are also a source of loss and often large in size. An ideal design would avoid intermediate or auxiliary components. The tag presented in this thesis differs from these currently proposed chipless RFID tags in that it relies solely on the scattering properties of a passive object and requires no supporting components.

Considering that at present, RFIDs employ a chip in their design, cost pennies a piece, and work; one might be tempted to ask "why bother with a chipless design?". We do not envision this concept of a chipless RFID replacing conventional RFIDs in commercial warehouses in the near future, but perhaps instead present in the vicinity of U.S. military ordinance where radiated energy is strictly controlled by Hazards of Electromagnetic Radiation to Ordnance (HERO) standards. This is perhaps the most dramatic benefit of a chipless RFID design; dramatically lower radiated power requirements. A significant problem with conventional chipped RFID tags is the need to be power-scavenging or self-powering. Power-scavenging is needed to energize a monolithic chip to start the tag reading process. A power -15 dBm at the chip terminals is a typical required power value. For obvious reasons, a chipless design does not have a turn-on power requirement, but instead is limited by the ability of the reader to detect the tag. This becomes a function of the radar cross section of the tag. To facilitate a comparison, consider that at a distance of 1 meter, a chipped RFID operating at 928 MHz would require 9.0 dBm of transmitted power just to energize the chip. This is assuming the tag reader has a 6 dBi patch antenna and the tag itself a 1.76 dBi dipole antenna. At the same distance with the same 6 dBi antenna on the reader and a receiver sensitivity of -100 dBm at 10 GHz, a chipless RFID requires -18.1 dBm of radiated power in order to

be detected. This is based on an assumed radar cross section of -30 dBsm which is the value predicted by simulation for the notched elliptical dipole tag. The chipless design requires ~9 dB less radiated power. The Federal Communication Commission (FCC) under section 15.247 limits a reader to 1 Watt of effective isotropic radiated power, which using the assumed parameters limits the chipped RFID tag to an absolute maximum range of 11.2 meters. Using the same 1 Watt ERIP limit, the chipless RFID tag would have a theoretical maximum range of 16.4 meters. In practice, both tags would have a shorter readable range than that predicted based solely on power requirements.

Another advantage in addition to less radiated power, is that a chipless RFID is more or less insensitive to environmental conditions. In theory, it will operate up until its structure is compromised. At temperatures where chips are rendered inoperable, a chipless RFID has no difficulties operating.

Potential answers to "why a chipless RFID" is anywhere where you have extreme environments or where minimal radiated power is required. We have the "why" of going chipless, so now we'll address the "what. What is a chipless RFID? The fact that the chip is eliminated is obvious from the name. The question then arises "how are we to store and retrieve data with no chip". This is the essence of the chipless RFID, a structure that when electromagnetically excited, scatters a unique signature containing the desired data. Data is thus encoded in the structure and retrieved from the scattered field.

The purpose of this thesis is not to present a mature chipless RFID design, but rather to investigate the feasibility of the chipless RFID, with specific emphasis on Singularity Expansion Method (SEM) based concepts. The result is a chipless RFID tag with complex frequency domain singularities as the method for encoding and retrieving data.

1.1 Executive Summary

To provide the motivation for considering an embedded singularity based tag Singularity Expansion Method theories (SEM) are first presented. The main point that comes out of SEM is that it is correct to characterize the scattering response of the tag with pole singularities. SEM predicts that the pole singularities are inherent to the

structure and independent of excitation and observation. The Matrix pencil algorithm with Singular Value Decomposition (SVD) based sorting was chosen to extract poles. The SVD sorting is shown to be useful for extracting poles in the presence of noise.

The notched elliptical dipole tag is presented as the chipless RFID that will be analyzed to explore a singularity based encoding scheme. It is a functioning RFID that was initially presented as having nulls in the frequency domain scattered fields. When consider in terms of pole singularities, a distinct pole signature is found. To affirm that the poles are attributable to the notch structures, a comprehensive study considers permutations of the tag involving selectively removing notches. The permutation study results in pole signatures for all permutations. The signatures indicate the presence or absence of each physical notch thus showing the ability to encode 3 bits in the form of singularities. Each pole is attributed to a specific notch or the base tag structure. The key result of this section is that a pole signature is determined that can be used to read the tag.

Next, simulations that vary the observation point and or the excitation incidence show that the poles are aspect independent. Poles exactly matching the ideal tag signature are extracted even with the aspect variations. Other poles not previously observed are also noted, and are projected to be either true poles inherent to the structure or curve fitting poles due to the complexity of the signal. Monostatic radar type simulations are also considered, and it shown that viable pole signatures can be extracted even with the tag on edge. However, the tag is not predicted to be readable when the exciting fields are cross-polarized.

The thesis culminates by taking a prototype tag and successfully extracting a pole signature. The measurement setup consists of two horn antennas with the tag placed bore-sight 1 meter away. Additional measurements and processing are required to remove coupling between the horns, background scattering, and deconvolve the response of the horns. An isolated tag response is reached, and a matching pole signature is extracted. The tag was successfully read via its complex plane singularities when both oriented normal to the antennas and also when on edge. As predicted by simulations, a valid pole signature was not extractable when the tag was cross-polarized.

1.2 Thesis Overview

This thesis consists of five chapters, with the bulk of the work being presented in Chapters 3 and 4. First SEM concepts that are applicable to the investigation are presented in Chapter 2. Chapter 3 considers simulations for the purposes of exploring embedded singularities. The main goal of this thesis is achieved in Chapter 4, where a prototype tag is successfully read via its pole signature. Chapter 5 presents a summary of the thesis, and suggests topics for future exploration.

CHAPTER 2

Singularity Expansion Method (SEM)

2.1 Origins of SEM

The original motivation for the Singularity Expansion Method dates back to the 1970s when it was introduced as a means for characterizing the electromagnetic response or scattering behavior of objects subjected to EMP phenomena [12-14]. It arises from practical observations noting that electromagnetic responses to impulsive excitations generally take the form of a summation of damped sinusoids. In the following sections, SEM concepts are briefly reviewed with most emphasis placed on the features and benefits of an SEM based approach to chipless RFID tags.

The basic premise of SEM is that an object's response to electromagnetic stimuli can be completely characterized by singularities in the complex frequency plane (the double sided Laplace transform plane). In terms of singularities, a damped sinusoid corresponds to a complex conjugate pair of pole singularities in the complex frequency plane. SEM results show that the pole singularity is sufficient to characterize the late time response of objects that are; finite in size, perfectly conducting or otherwise suitably constrained in their composition, and excited by a wave-form containing no branch- cuts [12]. Being that the chipless RFID tag considered in this thesis is a finite sized object and is constructed with simple dielectric and conducting materials; the pole singularity is of particular importance and is a suitable parameter to characterize the scattered fields. The

poles singularity is used for the purposes of this thesis. No other types of singularities are considered, and thus will not be detailed in the following sections.

2.2 Pole Singularities

A pole can be defined by a point location in the complex frequency plane. Poles are one of the more interesting singularities in the complex frequency domain because their physical significance in the time domain is immediately recognizable. A single complex conjugate pair of poles represents a damped sinusoid in the time domain. The pole location on the horizontal or real axis represents exponential growth or decay, specifically; the left half of the plane corresponds to a decaying sinusoid, and a location in the right hand plane represents an exponentially growing sinusoid. The vertical location on the imaginary axis is the frequency of the pole pair and the horizontal axis represents the damping portion of the exponential. Due to the fact that they represent a real signal in the time domain, poles must always be found in complex conjugate pairs, one being a positive frequency, and the other a negative frequency.

In the context of our intended application to chipless RFID tags, a passive scattering object, poles are limited to the left half of the complex frequency plane. This is attributable to the passive nature of the tags and the resulting decaying nature of any excited and observed scattering response. A set of poles in the right hand plane would indicate an exponentially growing response which is impossible for the late time response of a passive scattering object. In addition, a pole lying on the imaginary axis represents a sinusoid with no decay or growth. This would be a lossless scenario. In practice, some loss mechanism will always be present (radiation, Ohmic losses, etc.), and so no poles lying exactly on the imaginary axis should be observed.

An SEM type solution cast in terms of pole singularities would take the form of Equation 2.1. The solution has been expanded into a form where the pole singularities are only dependent on parameters of the object. The residue term, $R_i(\theta,\varphi)$, is dependent on the observation position, as well as the manner of excitation.

$$y(\theta,\varphi,t)=\sum_{i=1}^{M}R_i(\theta,\varphi)\cdot\exp(s_i\cdot t)\Leftrightarrow Y(\theta,\varphi,s)=\sum_{i=1}^{M}\frac{R_i(\theta,\varphi)}{s-s_i} \qquad \textbf{Equation 2.1}$$

Where

$y(t)=$ observed time response

$R_i=$ residues or complex amplitudes

$s=\alpha+j\cdot\omega$ complex frequency

$s_i=\alpha_i\pm j\cdot\omega_i$ poles

$\alpha_i=$ damping factors

$\omega_i=$ angular frequencies

2.3 An example set of poles in the frequency and time domain

As an example of a pole representation of a signal, consider the set of poles in Table 2.1. In the time domain, these poles represent a response consisting of a summation of damped sinusoids. Equation 2.2 shows the resulting signal starting with the frequency domain and ending with the corresponding time domain damped sinusoids.

Note that the all the damped sinusoids differ from each other in terms of magnitude, phase, damping, and frequency. The first pole residue pair, S_1 and R_1, is excited the strongest, has the highest damping, and the highest frequency. Looking at Figure 2.1, as would be expected it dominates initially and then decays. The remaining two poles become distinguishable later in time due to their lower damping. The phase differences and magnitude difference are immediately obvious at 0 s when considering each pole individually.

Table 2.1-Poles and Residue values to be used as an example throughout this section.

Residues	Poles
$R_1=11$	$s_1=1\pm 2\pi 2\mathrm{j}$
$R_2=7e^{j\frac{\pi}{2}}$	$s_2=2\pm 2\pi 3j$

$R_3 = 20e^{j\pi}$	$s_3 = 5 \pm 2\pi 12j$

$$\frac{11}{s-1+2\pi 2j}+\frac{11}{s-1-2\pi 2j}+\frac{7e^{j\frac{\pi}{2}}}{s-2+2\pi 3j}+$$

$$\frac{7e^{j\frac{\pi}{2}}}{s-2-2\pi 3j}+\frac{20e^{j\frac{\pi}{6}}}{s-5+2\pi 12j}+\frac{20e^{j\frac{\pi}{6}}}{s-5-2\pi 12j}$$

Equation 2.2

$$\Longleftrightarrow 11(e^{-(1+\mathrm{j}2\pi 2)t}+e^{-(1-\mathrm{j}2\pi 2)t})+7e^{j\frac{\pi}{2}}(e^{-(2+\mathrm{j}2\pi 3)t}+e^{-(2-\mathrm{j}2\pi 3)t})$$

$$+20e^{j\pi}(e^{-(5+\mathrm{j}2\pi 12)t}+e^{-(5-\mathrm{j}2\pi 12)t})$$

$$=22e^{-t}\cos(2\pi 2t)+14e^{-2t}\cos(2\pi 3t+\pi/2)+40e^{-5t}\cos(2\pi 12t+\pi)$$

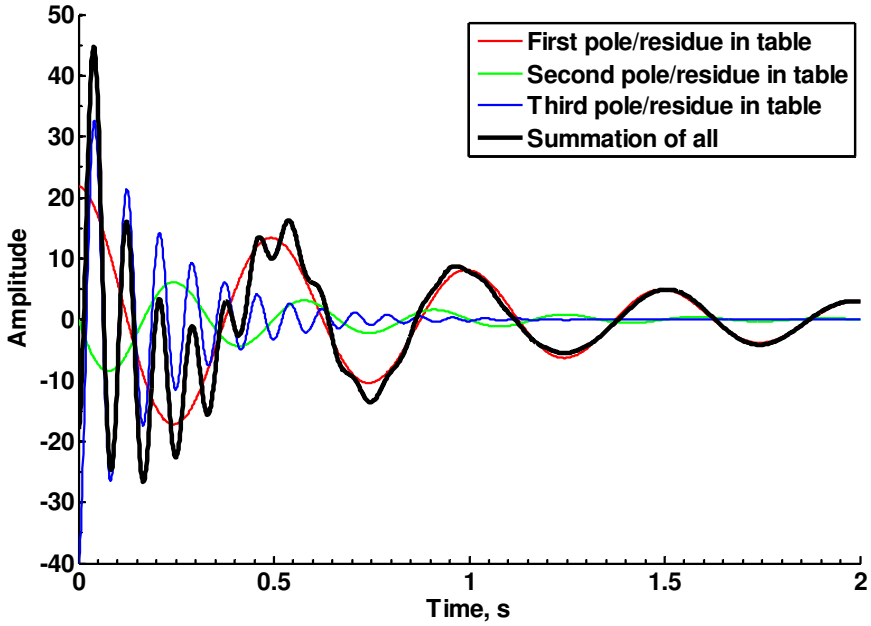

Figure 2.1-Time domain waveform represented by a summation of the poles in Table 2.1. The signal for each individual pole is also shown.

2.4 Aspect Independent Nature of SEM

One particularly useful property of an SEM based solution, specifically when poles are the singularity of interest, is that it can be manipulated into a factored form which separates the solution's dependencies on various parameters including features of the; incident field, observation location, and characteristics of the scattering body [15]. Most important for our purposes is that the pole singularities, specifically the pole location in the complex frequency plane, are found to be aspect independent and thus only dependent on the structure of the scattering body. "Aspect" is use throughout the thesis to refer to the manner in which any object is observed; mainly excitation incidence and observation position. The aspect independent nature was immediately recognized as particularly applicable for target identification purposes [16]. In essence, the process of creating a chipless RFID tag is a form of target identification with the exception that the target is now created in such a way as to be uniquely identifiable.

For the case of a chipless RFID tag, because it is a finite sized conducting object with suitably constrained material parameters, according to SEM the scattered fields can be characterized by pole singularities and associated residues. The pole singularities are inherent to the structure and represent the source free solution or natural oscillations. The poles are independent of the excitation as well as observation position. Because they are inherent to the structure, poles can be created and or manipulated by changing the structure. If a structure can be created or modified such that it has a distinct set of poles, the poles can be used as the parameters in which the data is encoded and thus retrieved. This is the basis for our chipless RFID concept; to create a structure with a distinct signature of embedded singularities that are retrievable via the scattered fields.

2.5 Why SEM?

For our purposes, SEM does not provide an analytical solution to our problem, nor does it provide a method for embedding singularities into a structure, or even a pole extraction algorithm for reading the pole signature. What it does provide, is the justification for choosing pole singularities as a valid and particularly suitable

representation for the scattering behavior of our chipless RFID tags and the inherent practicality of using a pole signature as a method for encoding and retrieving data.

2.6 Matrix Pencil Algorithm to Extract Poles

If we are to retrieve the data from a pole signature, we must first extract the poles from the scattered fields. This is accomplished by considering the scattered time domain waveform and using one of several methods for extracting poles. Prony's method is perhaps the first such method for extracting poles from a waveform, however it is unacceptably susceptible to noise to be practical [17]. For the work presented, we used Hua and Sarkar's Matrix pencil Algorithm which has a Singular Value Decomposition (SVD) sorting feature giving it the ability to cope with noise [18, 19]. We will not go into detail about the operation of the Matrix pencil algorithm. The references for this section explain its implementation.

2.6.1 Coping with Noise, SVD Sorting

The formulation of the Matrix Pencil algorithm as presented by Sarkar and Hua uses a Singular Value Decomposition (SVD) to sort the results. This is particularly useful because it provides a means to sort out and discard spurious poles resulting from noise under the assumption that noise poles will have relatively lower singular values. The SVD sorting parameter, p in Equation 2.1, is based on discarding all singular values that fall below a threshold when compared in a ratio to the maximum singular value. Hua and Sarker suggest a level for the sorting parameter based on the number of significant digits in the data under consideration.

$$\frac{\sigma_c}{\sigma_{max}} \approx 10^{-p} \qquad \textbf{Equation 2.3}$$

With the SVD sorting, a threshold of 30 dB is cited as being the minimum SNR to accurately extract poles [20]. In reality, accurate is defined based on the application. While 30 dB is singled out as being a minimum SNR, for our purposes of reading a tag

based on a pole signature, it is possible a lower SNR would still be usable. We are not developing a decoding algorithm, but rather going by a visual inspection of the results. Determining an actual SNR value to use as a rule is not possible. However, we will test the 30 dB SNR figure.

Consider the time domain waveforms of Figure 2.2. These are the example poles defined waveform as defined in Table 2.1 with varying degrees of added noise ranging from a 40 dB SNR to 10 dB SNR. If we apply the matrix pencil algorithm with SVD sorting to these waveforms, we obtain the pole sets as shown in Figure 2.3. The exact pole locations as defined for the example are indicated by the large circle markers with the center of the circle being the exact location of the pole. For all noise scenarios considered, all three poles were successfully extracted. In this case, "successfully extracted" means that we have a pole that by inspection falls close to the correct location and has an amplitude similar to that specified for the example.

As a comparison to show to what degree the parameters of the poles and residues were extracted successfully, consider Table 2.2. We will simply go straight to the worst case, and consider a signal to noise ratio of 10 dB. This is 20 dB below the minimum recommended SNR. The 3 Hz pole has the highest percent error of 2% for frequency and 11.2% off in damping. While 11.2% error sounds like a lot, without a decoding algorithm it is meaningless. Without a decoding algorithm, we rely on a visual inspection of the pole locations relative to a reference to interpret results, and by inspection the 3 Hz pole with an SNR of 10 dB is still readable.

This brief investigation was not intended to set an SNR limit for our application, but rather to point out that the 30 dB limit is most likely unnecessarily high. We were able to extract a potentially viable pole signature for a SNR as low as 10 dB.

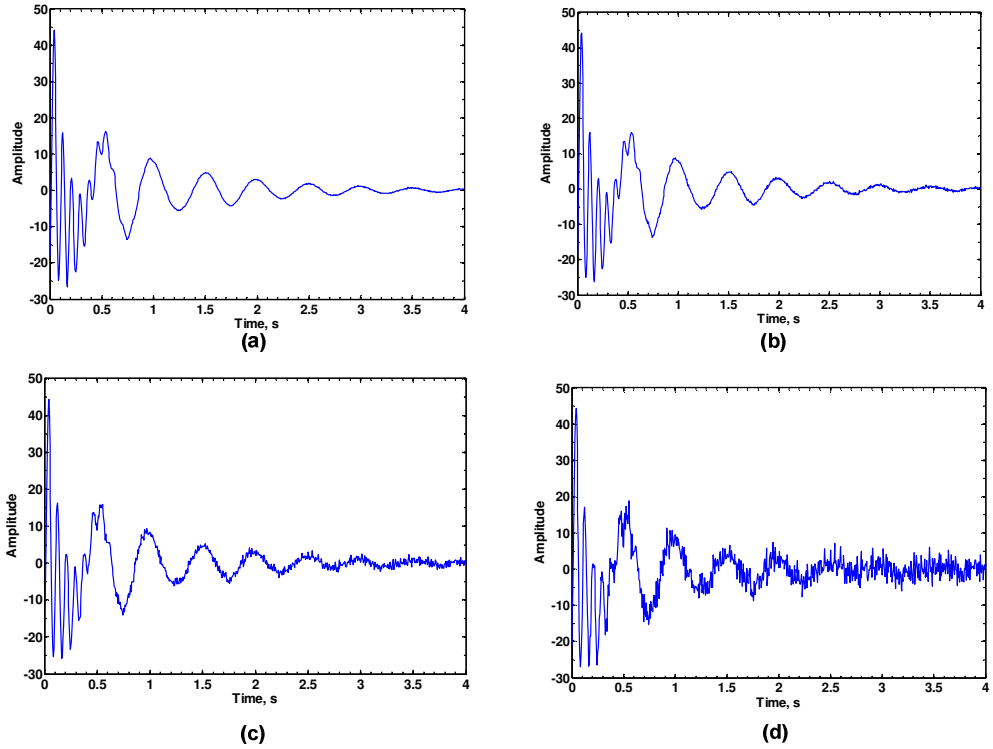

Figure 2.2-Time domain waveform defined by the poles and residues of Table 2.1 with noise added. a) SNR 40 dB, b) SNR 30 dB, c) SNR 20 dB, b) SNR 10 dB.

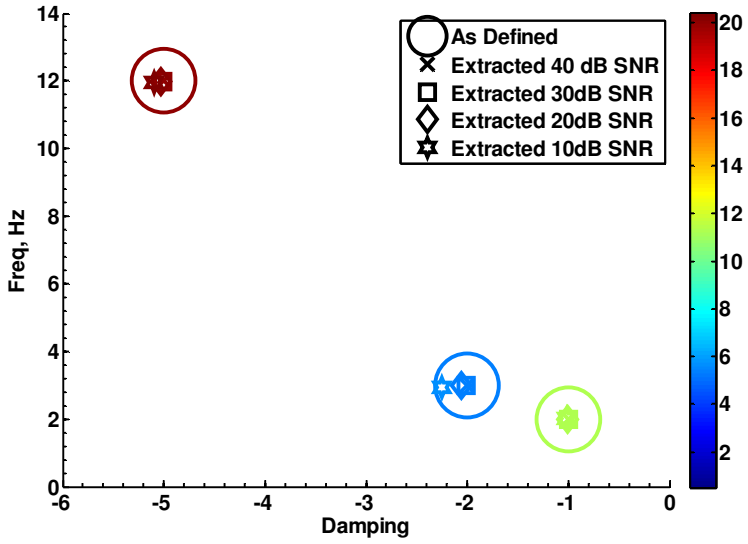

Figure 2.3-Poles extracted for the time domain waveforms of Figure 2.2 consisting of the example pole set with various levels of noise added.

Table 2.2-Comparison of the extracted poles and residues for various SNR for the example set in Table 2.1

	Pole Parameters						Residue Parameters						
	Frequency			Damping			Magnitude			Phase			
SNR, dB	Defined	Extracted	% error	Defined	Extracted	% error	Defined	Extracted	% error	Defined	Extracted	error	SVD Sorting Parameter
40	2.00	2.000	0.009	-1	-1.000	0.043	11	11.001	0.008	0.000	-0.001	0.001	2.000
	3.00	2.998	-0.050	-2	-2.005	0.241	5	5.003	0.054	1.571	1.574	-0.004	
	12.00	11.998	-0.016	-5	-5.003	0.068	20	20.012	0.058	3.142	3.143	-0.001	
30	2.00	2.001	0.029	-1	-1.001	0.140	11	11.003	0.028	0.000	0.003	-0.003	1.000
	3.00	2.995	-0.159	-2	-2.016	0.780	5	5.010	0.205	1.571	1.582	-0.011	
	12.00	11.994	-0.050	-5	-5.011	0.213	20	20.037	0.183	3.142	3.145	-0.004	
20	2.00	2.002	0.093	-1	-1.005	0.475	11	11.014	0.128	0.000	0.008	-0.008	0.900
	3.00	2.985	-0.516	-2	-2.055	2.670	5	5.051	1.000	1.571	1.607	-0.037	
	12.00	11.982	-0.153	-5	-5.033	0.655	20	20.115	0.574	3.142	3.152	-0.011	
10	2.00	2.006	0.314	-1	-1.022	2.175	11	11.140	1.257	0.000	0.030	-0.030	0.800
	3.00	2.941	-2.021	-2	-2.254	11.282	5	5.406	7.504	1.571	1.721	-0.150	
	12.00	11.949	-0.423	-5	-5.102	1.997	20	20.388	1.905	3.142	3.118	0.024	

How the SVD sorting was used

The Singular Value Decomposition (SVD) sorting feature of the Matrix-Pencil algorithm was implemented by starting with a value of 9, and iteratively running the Matrix-Pencil algorithm lowering the SVD parameter for successive runs until poles were extracted that matched the number of poles known to be in the signal. For the case of our example in this section, the number of poles was three, and the SVD sorting parameter values for 40 dB, 30 dB, 20 dB, and 10 dB were 2.0, 1.0, 0.9, and 0.8 respectively. This works for our purposes because we have the luxury of knowing how many poles we should have beforehand. The same situation exists when we move on to considering chipless RFID tags, and the SVD sorting featuring was utilized in the same manner.

2.7 Conclusion

In this chapter, we have shown that we can use pole singularities to represent a signal that takes on the form of a summation of damped sinusoids. This pole representation is suitable for characterizing the scattering response of our chipless RFID tags and is predicted by SEM theory to have properties that should prove useful. These properties are as follows; poles are inherent to the structure and can be manipulated by changing the structure, poles are aspect independent, and can be extracted via known algorithms that can cope with the presence of noise. An example of a pole set representing a damped sinusoidal signal was presented, and it was shown that the poles could be extracted from a time domain signal in the presence of noise with the Matrix-Pencil algorithm. The SVD sorting feature of the Matrix-Pencil algorithm was shown to be useful for removing the number of spurious noise created poles.

CHAPTER 3

Notched Elliptical Dipole Tag

Recall that the goal of this thesis is not to develop a chipless RFID design, but rather to investigate the use of SEM based concepts. In order to explore the concept of using embedded singularities as a data encoding method as well as a mechanism for retrieval, this section considers both simulations and measurements of an existing chipless RFID tag, the notched elliptical dipole.

3.1 Origin of the Notched Elliptical Dipole Tag

A concept for a chipless RFID based solely on the scattering properties of an object was proposed by Manteghi and Rahmat-Samii [10]. In their paper, they described their chipless RFID as a "Notched Elliptical Dipole Tag with multi-bit data scattering properties". The subject of their paper, the notched planar elliptical dipole tag, is a planar scattering body which originated as a modification of an existing antenna design [21]. The notched elliptical dipole tag, as pictured in Figure 3.1, has no chips, transmissions line, auxiliary antennas, or other discrete components present.

The premise of their work was that they were able to create nulls in the radar cross section spectrum of the tag by creating physical notches in the structure. Each null was regarded as a bit of data, giving the tag 3 bits of data storage. As an initial simplistic decoding algorithm, the presence of a null would be interpreted as a 1, and the absence of null as a 0. They only considered the tag with three notches present, and the radar cross section spectrum was considered as the scattered field parameter of interest. The radar cross section spectrum they observed took the form of Figure 3.2, and the nulls corresponding to the encoded bits are evident at 6.5, 8, and 9.5 GHz.

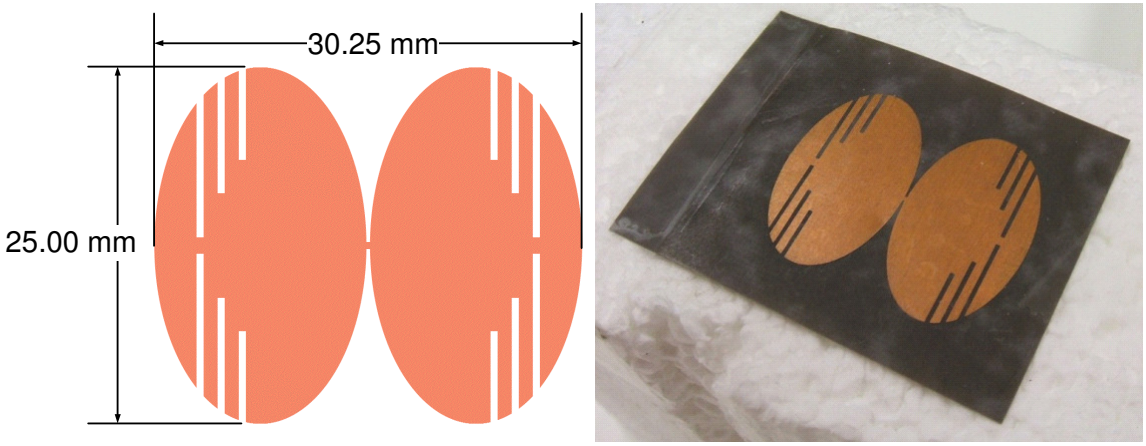

Figure 3.1-Notched Elliptical Dipole Tag. (a) Dimensioned (b) Prototype tag used for measurements.

The notched elliptical dipole tag is a working chipless RFID, and serves as the basis for a large portion of this thesis. First, simulations of the notched elliptical dipole tag's scattered fields will be considered to gain insight into the behavior of a chipless RFID tag when considered in terms of embedded singularities. Initially the simulations will retrace the results presented in the original journal article and then proceed to the singularity based analysis. Retracing previous work is seemingly redundant, but it serves to validate the FEKO™ simulations and is necessary to build up to the SEM based analysis. The methodology developed while considering simulation results will lead directly to the next step of considering measured results. The ultimate goal is to sucessfully read a real embedded singularity tag, and this is the focus of the the conclusion of this section.

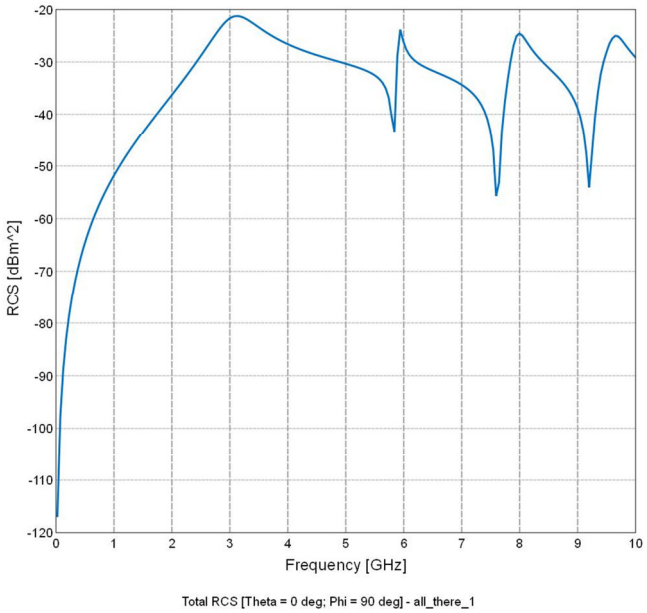

Figure 3.2-RCS of the notched elliptical dipole tag.

3.2 Simulating the scattered fields

We start by using simulation to examine the scattering behavior of the notched planar elliptical dipole tag shown in Figure 3.1. The ultimate goal is to present an SEM based analysis, but first we must have something to analyze. The first step is to verify that the simulation results agree with the results of Manteghi and Rahmat-Samii and proceed from there.

The scattered fields of the tag were simulated in FEKO™, a full wave simulator based on the method of moments. The simulation was run over 802 frequencies from 25 MHz to 20.05 GHZ with 25 MHz steps between points. The tag was assumed to have zero response at 0 MHz. In order to facilitate comparison to measured results, a dielectric of thickness 0.127mm, $\varepsilon_r = 2.20$, and $\delta = 0.001$ was incorporated in selected simulations. These parameters were chosen to match the RT Duroid 5880 material that the prototype tag used for measurements was fabricated on. When investigating permutations of the tag's structure, the dielectric substrate is omitted to expedite the simulation time as the presence or absence of a dielectric was not found to significantly alter the tag's behavior. In fact, the dielectric is only included when the simulation directly corresponds to a

measurement. Without a dielectric substrate, the tag is simulated as simply the metallic portion floating in free space. The expected differences between a dielectric substrate and a free space simulation in the frequency domain are a shift in frequency related to the relative permittivity of the dielectric substrate and in the time domain a change in damping due to the absence of loss in the dielectric. A less damped waveform is expected with the omission of the dielectric substrate. However, these differences are expected to be limited due to the thinness of the substrate and the fact that the tag is not fully enclosed by the substrate.

Excitation for all simulations is in the form of an incident plane wave. The ideal excitation to elicit the desired response of the tag with notches present is a plane wave normally incident to the surface of the tag, polarized such that the electric field component is in line with the minor axis of the tag's constitutive ellipses.

The parameter of interest is the scattered electric field sampled at a point in space. This metric is indicative of the RCS spectrum parameter, shown in Figure 3.2, considered by Manteghi and Rahmat-Samii [10]. When considered magnitude squared in log scale is considered, this parameter is equivalent to scattered power normalized to incident power. For a discussion of this, refer to Appendix A.

To facilitate discussion of variations in excitation (incidence and polarization) as well as observation, we will define a coordinate system. The coordinate system shown in Figure 3.3 will be used throughout for both simulation and measurement results. The coordinate system is defined based on the assumption that the coordinate system remains fixed to the tag and the exciting plane wave's direction of incidence and polarization changes. The coordinate system is defined as a Cartesian system with the x and y axes lying in the plane of the tag. The x axis is in line with the minor axes of the two ellipsis which form the body of the tag. The y axis is in line with the major axes of the two constitutive ellipsis. The z axis is the surface normal of the tag. When a dielectric substrate is present, the positive z direction indicates the side on which the metallic tag is located. The origin is located at the center of the tag.

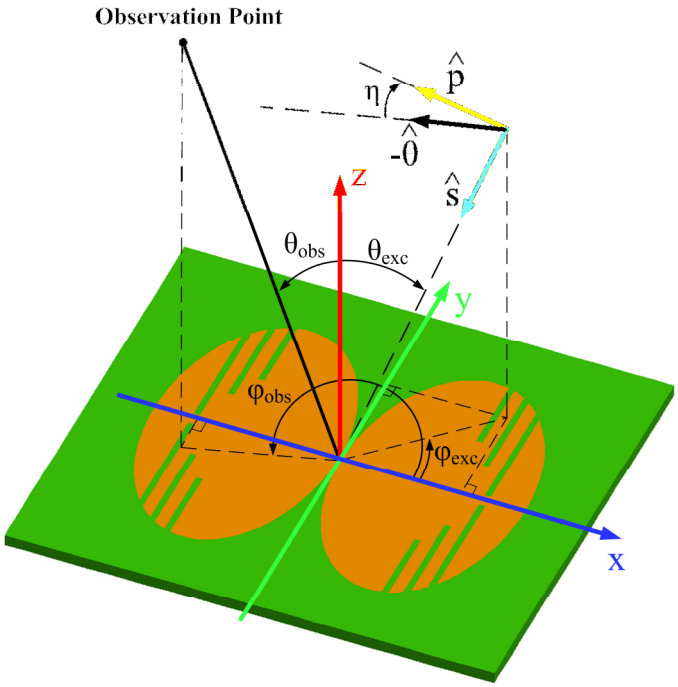

Figure 3.3-Coordinate System used to define excitation incidence and points of observation.

To define the incident plane wave, spherical coordinates will be used based on the previously defined Cartesian system. A plane wave can be characterized by two vectors which define the direction of propagation and the polarization. Throughout this thesis, the direction of incidence will be defined by an $\hat{s}$ vector. In terms of spherical coordinates, $\hat{s}$ is equal to $-\hat{r}$, and is completely characterized by θ and φ. Thus, when specifying the incidence of the plane wave, it will be given in terms of θ_{exc} and φ_{exc}. A normally incident plane wave would be specified as $\theta_{exc} = 0°$. This is equivalent to $\hat{s} = -\hat{z}$. The polarization of the incident plane wave's electric field is defined by the vector $\hat{p}$. In terms of spherical coordinates, $\hat{p}$ is defined by an angle, η, relative to the $-\hat{\theta}$ vector. Due to the nature of a plane wave and the manner in which we have defined our coordinate system, $\hat{p}$ will always be compromised of the $\hat{\theta}$ and $\hat{\varphi}$ vectors as follows $\hat{p} = -\cos(\eta) \cdot \hat{\theta} - \sin(\eta) \cdot \hat{\phi}$.

As an example of the use of the coordinate system consider the following: the ideal orientation of the tag to elicit the desired scattered response is $\hat{s} = -\hat{z}$, and $\hat{p} = -\hat{x}$. In terms of spherical coordinates this is $\theta_{exc} = 0°$, $\varphi_{exc} = 0°$, and $\eta = 90°$. This corresponds to a plane wave normally incident to the tag with the electric field polarized along the minor axes of the constitutive ellipsis forming the main body of the tag. If the observation point is considered to be located on the z axis, this is one of the cases considered by Manteghi and Rahmat-Samii, and will be the initial case considered for both measurements and simulations [10]. The point of observation will also be defined in terms of spherical coordinate using $\theta_{obs}, \varphi_{obs}$, and also an observation distance, r. To distinguish between excitation and observation parameters, excitation parameters will have a subscript "exc", and observation parameters will have a subscript "obs".

3.2.1 Tag orientations to be considered

There are infinite combinations of excitation incidences and observation directions that could be considered. We will restrict our investigation to a handful. Naturally, scenarios will be selected based on suitability to explore topics of interest which includes the intricacies, benefits, and limitations of an SEM based analysis, as well as features of the tag itself. Cases where the observation point is collocated with the source of the plane wave will be considered as they could be a possible reader configuration and model the measurements that are considered later. To clarify, collocated with the plane wave source means that the observation point lies on the axis defined by the $\hat{s}$ vector which defines the incidence of the exciting plane wave or in terms of our coordinate system $\theta_{exc} = \theta_{obs}$ and $\varphi_{exc} = \varphi_{obs}$. All variations considered are listed and categorized in Table 3.1. The following paragraphs summarize the scenarios selected and their intended purpose.

Ideal Case

First, we define an ideal case of a normally incident $\hat{x}$ polarized plane wave with the observation point located on the axis defined by $\hat{s}$, the direction of propagation of the incident plane wave. In terms of the coordinate system defined in Figure 3.3, this

corresponds to $\theta_{exc} = 0°$, $\varphi_{exc} = 90°$, $\eta = 90°$, $\theta_{obs} = 0°$, $\varphi_{obs} = 0°$, $r = 1\ m$. This case will always be referred to as the "ideal" case. It will serve as our starting point for going to an SEM based analysis. It also forms the basis for comparison for all other cases. The results of this ideal case are considered to be the signature of the tag. This is also the scenario used when considering permutations of the tag structure.

Monostatic Radar

Next, we will consider variations in excitation with the observation point held to be consistent with excitation $\theta_{exc} = \theta_{obs}$ and $\varphi_{exc} = \varphi_{obs}$. The ideal case detailed in the previous paragraph falls under this category. In practical terms such as a measurement setup or a tag reader, this would be equivalent to having the excitation antenna and receiving antenna collocated similar to a monostatic radar. In fact, the measurement setup and results considered later in this thesis use this configuration which is the main reason it is of interest. Not all of the simulation variations of this form considered were measured. Four cases were selected for measurements. Those selected for measurement are indicated by a "yes" in the "Measured" column of Table 3.1.

Non-ideal Excitation and Non-Ideal Observation, Bistatic Radar

The final variation in scenarios considered are those that involve either an excitation that deviates from the ideal case and or an observation point that is not collocated with the excitation source. These cases are intended to explore the aspect independent nature of the pole singularities predicted by SEM as well as possible quirks of the notched elliptical dipole tag. Only two cases are considered to try to limit the resulting information to a manageable amount. One case retains the ideal excitation of a normally incident x polarized plane wave, but does not have a collocated observation point. The other case involves a non-normal excitation and an non normal observation point.

Table 3.1-List of all combinations of excitation incidence and point of observation considered.

Notches	Θ_{exc}	Φ_{exc}	η	Θ_{obs}	Φ_{obs}	r	Measured	Comments
All Present	0°	90°	90°	0°	90°	1 m	Yes	Ideal Case
Permutations	0°	90°	90°	0°	90°	1 m	No	Ideal Case
All Present	0°	0°	90°	0°	0°	1 m	No	Normal Cross-polarized
All Present	90°	90°	90°	90°	90°	1 m	Yes	On edge Co-polarized
All Present	90°	0°	90°	90°	0°	1 m	Yes	On edge Cross-polarized
All Present	0°	0°	90°	45°	45°	1 m	No	Ideal Excitation Non-ideal Observation
All Present	45°	45°	90°	45°	225°	1 m	No	Non-ideal Excitation Non-ideal Observation

3.3 Simulation Results in the Frequency Domain

Now that we have a simulation setup and a coordinate system setup to define the cases being considered, we move on to consider some simulation results. We will first analyze the ideal case as this case represents the standard for comparison for all other cases. The process of achieving a pole signature for the ideal case will be shown in detail. For other cases, only the initial frequency domain simulation results and the final pole signature extracted will be presented in the main text. The results of the intermediate steps, specifically the plots of various waveforms, are omitted.

3.3.1 Ideal case in the frequency domain

The direct results of the FEKO simulation of the ideal case can be seen in Figure 3.4. The parameter being consider is the x polarized portion of the scattered fields at an observation point located normal to the surface. Initially, the tag behaves like a standard scattering body with the scattered fields increasing in magnitude as the excitation approaches frequencies where the tag dimensions are on the order of a wavelength. The physical notches are 6.32 mm, 7.95 mm, and 9.74 mm in length. They are a half wavelength slot cut in the middle, and thus are quarter wave resonant structures. In free

space assuming quarter wavelength resonance, from shortest to longest, the notch lengths correspond to frequencies of 11.87 GHz, 9.44 GHz, and 7.70 GHz. In reality, these frequencies will be higher than those at which resonant behaviors are observed due to two factors; the notches have a width and thus an effective length that is longer, and the presence of a dielectric substrate. Figure 3.4 shows simulations for both the case of the metallic tag in free space and also on a dielectric substrate. For the tag in free space three nulls are clearly evident at 6.0 GHz, 7.9 GHz, and 9.5 GHz. Recall that the dielectric substrate had parameters of; thickness = 0.127mm, ε_r = 2.20, and δ = 0.001. Comparing the scattered response with and without a dielectric substrate in Figure 3.4, shows that the addition of the dielectric substrate shifts the three nulls lower in frequency to 5.8 GHz, 7.3 GHz, and 8.8 GHz or a shift of 0.2 GHz, 0.6 GHz, and 0.7 GHz respectively. This shift is considerably less than what would be predicted by the relative permittivity of the dielectric. In reality, the frequency shift due to the dielectric is limited because the near fields associated with each slot are not contained completely within in the dielectric substrate. For this reason, the dielectric can be omitted without fear of altering the form of the tag response.

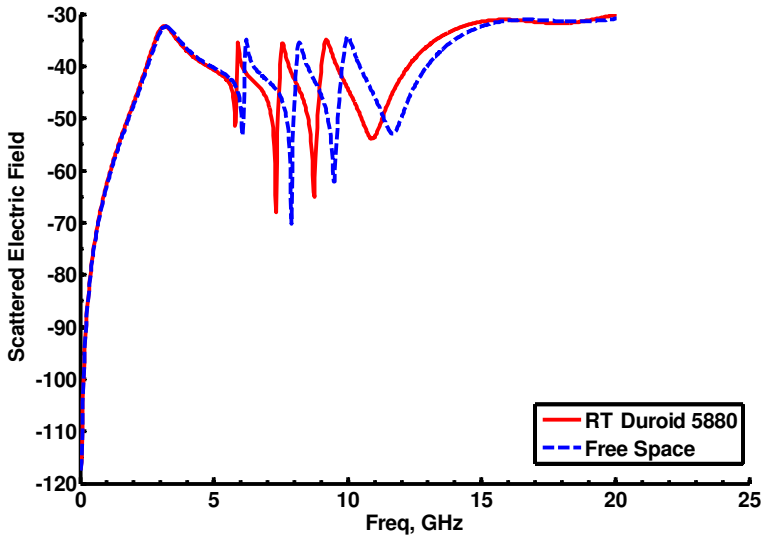

Figure 3.4-Scattered Electric Field as simulated in FEKO™ for the case of $\theta_{exc} = 0°, \varphi_{exc} = 0°, \eta = 90°, \theta_{obs} = 0°, \varphi_{obs} = 0°, r = 1\ m$ with and without a dielectric substrate with thickness of 0.127mm, ε_r = 2.20, and δ = 0.001

In the notched elliptical dipole tag, we have a structure with distinct, intentionally placed, physical features that create observable characteristics in the scattering response. If we consider the presence or absence of these nulls to correspond to encoded data, the notched elliptical dipoles tag is a functional chipless RFID with 3 bits of data. The data is retrievable from the scattered fields. The next logical thing to do if proceeding with a frequency domain analysis would be to consider other scenarios involving excitation and observation, and then perhaps move on to tag physical permutations. Rather than proceeding in such an incremental manner, we will go directly to an SEM based analysis involving singularities and consider frequency domain results as needed.

3.4 Tag response in terms of SEM

In the previous section, we were able to observe the effect of the notches in the frequency domain form of the scattered field. If the data can be recovered from the frequency domain response, what is the advantage of a singularity based analysis? By considering a pole signature rather than interpreting the frequency domain response, we are analyzing discrete parameters rather than interpreting a continuous curve. Due to the nature of poles, they do not change in location due to changes in observation position, and or excitation. This is the aspect independent nature referred to by Baum in his work with SEM. If we consider the presence or absence of a particular pole as a 1 or 0 respectively, and thus a bit of data, we have an easily interpretable discrete parameter for encoding and retrieving data that is tolerant of changes in excitation and observation.

Considering a signature which is based on pole location (damping, frequency) as the encoding scheme is the most simplistic approach. In general, a pole singularity and associated residue contain four pieces of information; frequency, damping, phase, and magnitude. While the pole, damping and frequency, is aspect independent, the residue is not. It is beyond the scope of this thesis, but future work could implement a more complex encoding scheme, and address the utility of these additional parameters. Using all four available parameters associated with each pair of poles, an embedded singularity tag in addition to being an RFID tag, has the potential to act as a remote sensor, detecting; rotations, translation, deformations, and possibly more.

3.4.1 FFT to the time domain

The Matrix Pencil algorithm as used in this thesis operates on time domain signals. The time domain waveform was generated by using the Matlab IFFT function on the frequency domain response generated by the FEKO simulations. Before doing the IFFT operation, the data was windowed using a raised-cosine function and also zero-padded. The windowing can conceptually be regarded as modifying the excitation waveform. The frequency domain windowing used has the effect of decreasing the duration of the impulse it represents in the time domain. The zero-padding has the effect of interpolating points in the time domain. The end result is a time-domain response to an impulsive excitation.

In reality, we are not interested in looking directly at the time domain waveform. However, a couple of observations are worth noting. First, note that the resulting time-domain form of the tag response seen in Figure 3.5 by inspection appears to consist of a summation of damped sinusoids suggesting that a pole singularity characterization is appropriate.

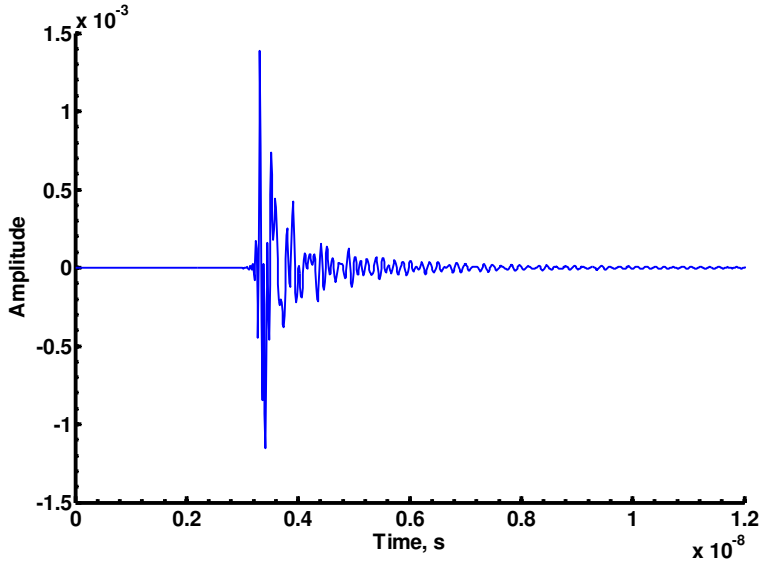

Figure 3.5-Simulated time domain response of the notched elliptical dipole tag

Second, in the simulation, the observation point was specified at a distance of 1 meter from tag. This distance corresponds to a propagation time of 3.33 ns in free-space. Fields scattered from the tag should not be observed earlier than this time. Looking at Figure 3.5, the onset of the observed response does appear to occur at ~3.33 ns. The utility of knowing the earliest time at which the scattering response could be observed becomes evident in the next section.

At this point, we have a time domain signal that we could pass to the Matrix Pencil algorithm. However, we must first choose which portion of the response we wish to consider.

3.4.2 Time Windowing

The time-domain form of the simulation results represent the tag's scattered response to an impulsive plane wave illumination. Due to the truncation of the frequency domain data, the incident plane wave is not an ideal impulse, and thus the excitation has some duration. For this reason, it is necessary to consider a section of the time domain signal that is sufficiently later in time than the initial observation of the onset of the excitation at 3.33 ns. This ensures that the tag response is being considered rather than the excitation. Due to the absence of noise in the simulations, the poles can be extracted from a time-window much later in time than would be possible in practice. If noise were present, a signal consisting of decaying sinusoids would eventually be indistinguishable from noise. For the simulation results, the most important consideration when applying a time window is the starting point such that it is sufficiently later in time from the onset of the excitation. As long as this criterion is met, the simulated results are not sensitive to choice of time-window.

As an example of a time window with too early a start time, consider Figure 3.6. The time window begins at 3.33 ns. The excitation is present in the early part of this time window. Performing a matrix pencil operations results in no valid poles returned. For the Matrix Pencil algorithm to work, the signal being considered must be representable by damped sinusoids in the form of poles singularities. When under the influence of a forcing function, SEM theory states that an entire function is needed to characterize the

response. Thus, when a forcing function is present, a pole singularity representation is not valid. We are only interested in the source free response of the tag and a pole singularity representation, and so a section of the response must be selected that is later in time than the onset of the excitation.

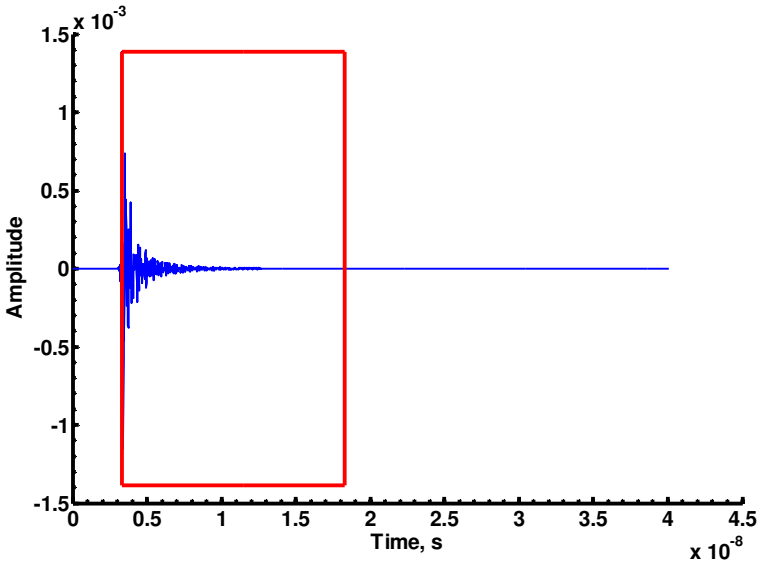

Figure 3.6-Example of too early a time window indicated by the red box. The time window starts at 3.33 ns, the earliest time any observed response should be observed based on an observation distance of 1 m.

For most cases, a suitable time window was determined for each scenario based on inspecting the time-domain waveform to determine the beginning of the response, and then experimentally altering the start of the time window and the length. The window start time was deemed acceptably late time when the same poles could be extracted repeatedly for subsequent windows with later start times. For the simulations, one window was found to work for most scenarios considered. A start time of 3.7 ns was found to be generally suitable.

The remaining parameter needed to specify the time window is the duration of the window. In our case, knowledge of the object of interest's physical nature is known, and thus the lowest expected frequency poles are predictable. Using this knowledge, the duration of the time window was set such that it would include at the minimum several cycles of the lowest expected frequency of interest. Looking at the frequency domain

scattered response in Figure 3.4, the tag's lowest frequency feature in the scattered response peaks at ~3 GHz. Assuming that the lowest frequency poles should occur around this peak, we will use 3 GHz to calculate the time window durations. Using 20 cycles of a 3 GHz sinusoid corresponds to a duration of 6.7 ns. With this last parameter we have the time window used for the simulations; a start time of 3.7 ns and ending 6.7 ns later at 10.4 ns.

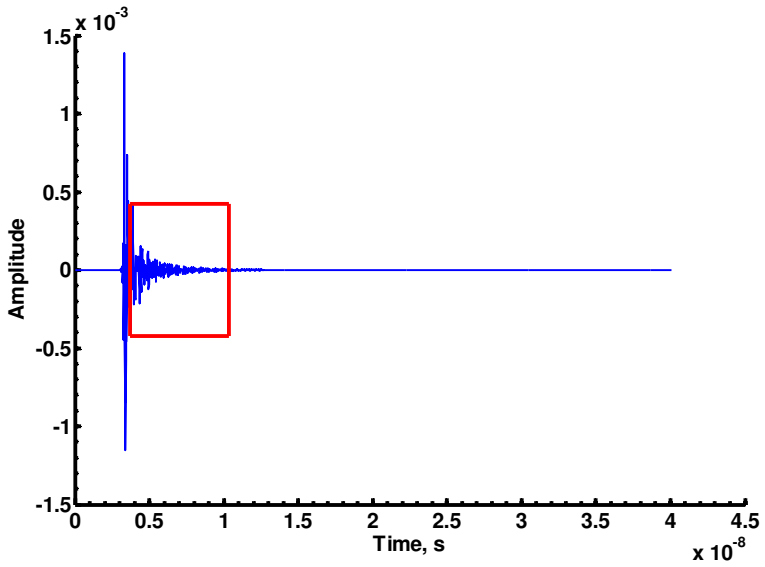

Figure 3.7-Time domain form of the scattered electric field for the ideal case showing time window used for all simulation results. The time window is indicated by the red rectangular box. Start-time = 3.7 ns and end-time = 10.4 ns

Is SVD sorting needed with no noise present?

Recall that when discussing time windowing it was pointed out that we do not have noise in the simulations. The SVD sorting feature of the Matrix pencil algorithm is primarily intended to cope with noise. However, it can also be used to limit the number of poles returned. This is necessary for simulations even without the presence of noise due to the limited number of digits. In effect, we have noise due to rounding. Even if we were able to extract every single pole accurately this is not necessarily desirable. In reality, we are interested in what one might call the dominant or significant poles of the structure. The SVD sorting parameter serves to restrict our attention to these dominant poles. The

SVD sorting was used for every case, but unless intentionally lowered for a purpose it is not mentioned. A sorting parameter of $p = 8$ was used for all simulation results unless otherwise noted.

3.4.3 Pole Signature of the Tag

The time window of Figure 3.7 indicated by the rectangular box has the earliest start time found to be sufficiently later than the time of excitation onset. Using this section of the time domain response with the Matrix Pencil algorithm, the set of poles of Figure 3.8 were extracted.

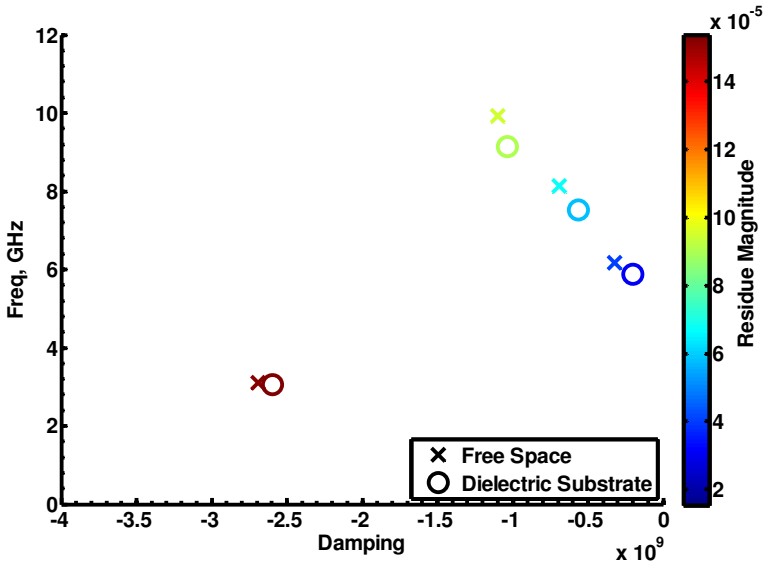

Figure 3.8-Pole signature of the notched elliptical dipole tag for the ideal case. Results are show for both the metallic portion in free space and on a dielectric substrate.

This set of four poles is the tag signature and is consistently extracted for time windows starting at 3.3. For the tag in free space, the three poles at 6.2, 8.1, and 9.9 GHz are attributable to the notches. This is validated in section 3.5 by selectively removing notches from the structure and noting that the presence or absence of a particular pole corresponds to a particular notch. The pole at 3.1 GHz was present for all combinations of notches including the tag structure with no notches. This indicates that the 3.1 GHz

pole is inherent to the base dipole tag structure. These four poles are the signature of the elliptical dipole tag with all notches present. Now that we have a pole signature for the tag from simulation, exciting the tag with incident fields from an antenna, measuring the fields scattered from the tag, and then extracting a matching pole signature would mean that we have successfully read the tag. This is the ultimate goal of this section: to successfully read an actual tag.

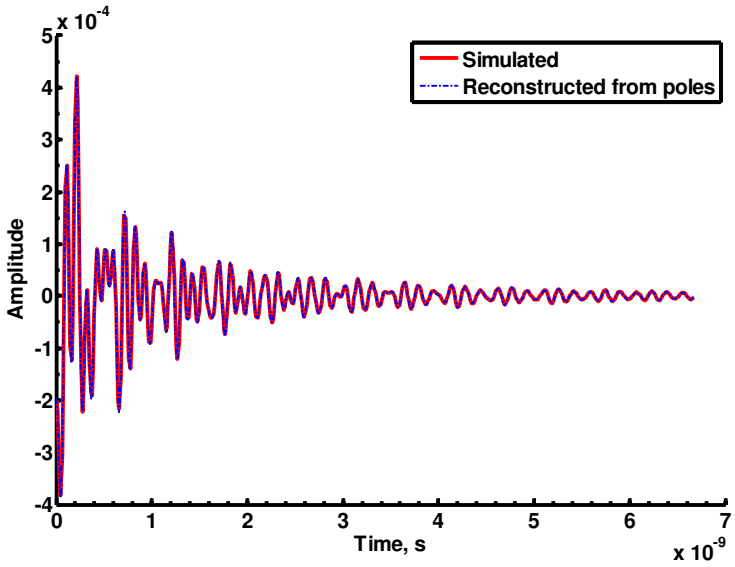

Figure 3.9-Time domain scattered response of the notched elliptical dipole reconstructed from extracted poles compared to the original response

3.4.4 Curve fit or Natural Oscillations?

The argument could be made that the poles are simply a curve fit rather than the true poles of the structure (natural oscillations). Consider Figure 3.9, which compares the time domain signal represented by the extracted poles to the original signal. The reconstructed signal is in fact a very good fit to the original signal, but it does not prove that the poles are attributable to physical features of the tag and are thus natural oscillations.

If the poles are in fact natural source free oscillations, they should correspond to a physical feature of the tag. In our case, the notches are the physical feature of interest and are considered to be the source of three of the four poles as the pole location on the

frequency axis is similar to the resonant length of the notches. Another way to verify the assumption that three of the poles are attributable the three notches is to selectively remove the notches and observe the changes in the pole signature of the tag. The process of selectively removing notches and noting the presence or absence of a particular pole would indicate that the specific poles are attributable to a particular structure and thus not simply a curve fit. To this end, the next section considers physical permutations of the tag which selectively remove the notches.

3.5 Tag Permutations

In this section, we will explore all possible physical permutations of the tag consisting of the absence or presence of a notch. Considering these permutations is intended to verify that the pole signature presented in Figure 3.8 is in fact due to natural oscillations of the tag structure, specifically the notches. However, considering these permutations is also of interest because they lend some insight into the actual practical implementation of the tag. The most obvious way of encoding a bit of data is either removing or shorting a notch. If we consider the presence of a notch as a 1, and the absence as 0, the tag has three bits. We will consider the highest frequency notch to be the most significant bit, the middle frequency notch as the middle bit, and the lowest frequency notch as the least significant bit.

All permutations considered are pictured in Figure 3.10. To limit this investigation to a reasonable extent, only one form of excitation, the case of a normally incident co-polarized (the ideal case) plane wave, will be considered ($\theta_{exc} = \theta_{obs} = 0°$, $\varphi_{exc} = \varphi_{obs} = 0°$, $\eta = 90\,°$, and $r = 1\ m$). The simulations were run with the tag in free space.

The steps in processing the permutation simulation results in order to reach a pole signature are the same as presented for the ideal case in Section 3.4. The intermediate step plots do not provide any needed information for this exploration, and as a result, they are not described or presented. Only the frequency domain response and the extracted pole signature will be presented and considered in the main text.

As one reads this section, it quickly becomes evident that the poles do not act independently of each other. This was not unexpected. Ultimately, we are interested in reading a tag via its pole signature. Because we do not have a well-defined algorithm for doing this and do not intended to develop one, a decision regarding the readability for the resulting pole signatures for each permutation will not be presented on an individual basis. Instead, this is reserved for the conclusion of this section where all results can be considered as a group.

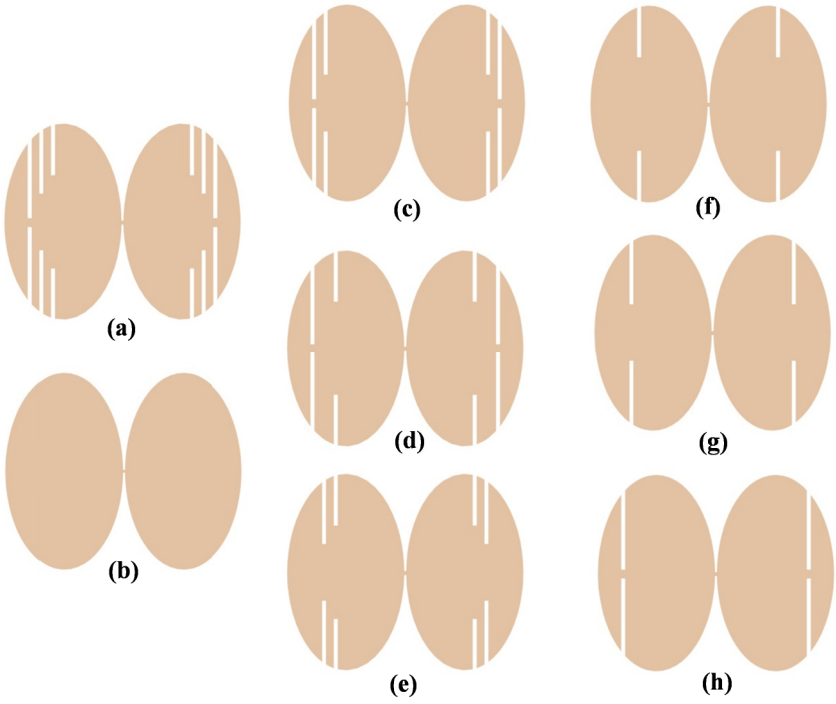

Figure 3.10-All permutations of the elliptical dipole tag considered. The binary bit sequence the permutation represents is listed after the description a) All three notches present 111 b) all notches removed, 000 c) middle and low present, 011 d) high and low present, 101 e) high and middle present, 110 f) high present, 100 g) middle present, 010 h) low present, 001.

3.5.1 No notches present

We will first consider the case with all of the notches removed. This permutation could be regarded as having binary 000 encoded. Any poles observed would have to be

attributable to the base dipole tag structure as no notches are present. The base dipole structure is a constant throughout the permutations, and any poles inherent to it should be observed for all variations.

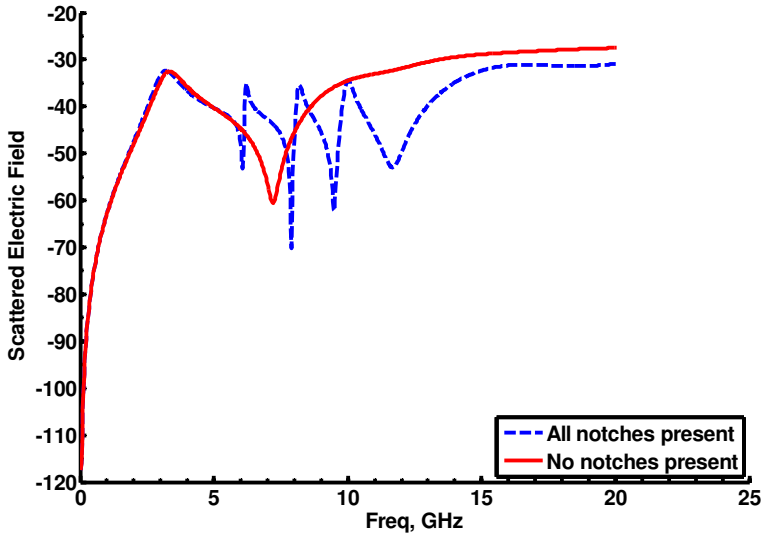

Figure 3.11-Scattered Electric Fields of the notched elliptical dipole tag with all notches removed.

First, consider the frequency domain form of the scattered fields in Figure 3.11. The three nulls at 6.0, 7.9, and 9.5 GHz that were attributed to the notches are now absent. There is a null present at 7 GHz which has to be attributable to the base structure. This null resembles the null that for the case with all notches present that was located at 12 GHz. It appears that removing the notches has had the effect of shifting this null lower in frequency. This is possibly attributable to the fact that the notches have the effect of dividing the base dipole structure into smaller pieces, thus when present shifting behaviors towards higher frequencies.

Based on the difference in the frequency domain, specifically the absence of features (nulls and peaks), we would expect that some poles would now be absent. Looking at the pole signature in Figure 3.12 we have one pole located at 3.2 GHz. Comparing this pole signature to that of our ideal case signature in Figure 3.8, we see that the three poles at 6.2, 8.1, and 9.9 GHz are now absent which would seem to indicate they were due to the now absent notches. While not exactly the same in location, the pole

at 3.2 GHz is close to the 3.1 GHz pole present in the ideal case pole signature. This suggests that the ideal case pole at 3.1 GHz and the 3.2 GHz pole are the same pole inherent to the base elliptical dipole structure.

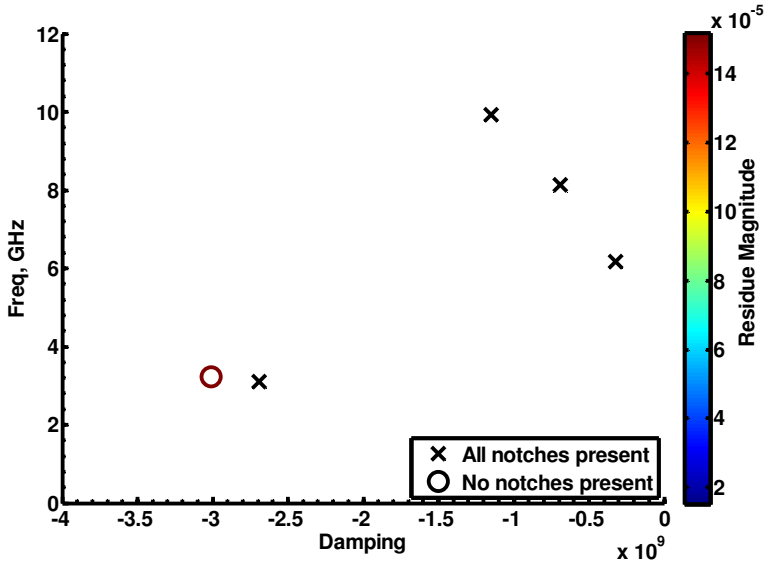

Figure 3.12-Pole signature of the notched elliptical dipole tag with all notches removed.

3.5.2 Middle and Lowest Present

In this permutation, the highest frequency notch is removed, leaving only the middle and lowest frequency notches. This permutation could be regarded as having binary 011 encoded. Looking at the frequency domain form of the scattered fields in Figure 3.13 reveals that the highest frequency null is also gone. The middle and lowest frequency nulls are still present but appear shifted slightly lower in frequency. This indicates that the middle and lowest frequency notches behave for the most part independently of the high frequency notch.

Looking at the pole signature of Figure 3.14 reveals that the highest frequency pole at 9.9 GHz is now absent. This indicates that the pole at 9.9 GHz is attributable to the highest frequency notch. It was noted in the frequency domain that the null locations for the remaining two notches were shifted slightly lower in frequency. This effect can also be seen in a slight frequency shift for the two poles at 6.2 and 8.1 GHz. Most likely

this amount of shift in frequency would not be problematic when developing a tag reading algorithm.

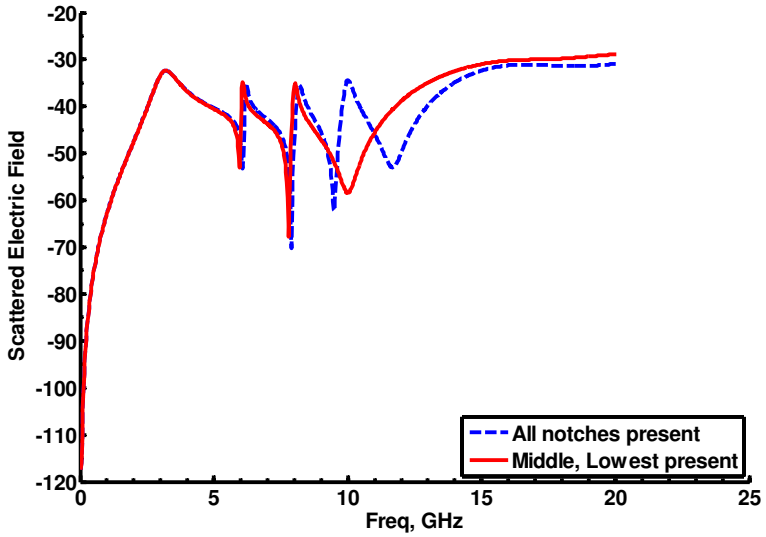

Figure 3.13-Simulated Scattered Electric Fields of the notched elliptical dipole tag with the highest frequency notch removed.

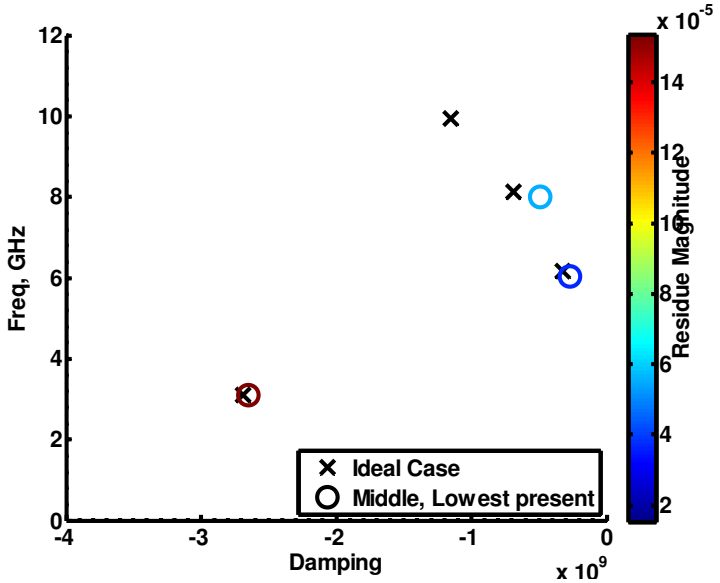

Figure 3.14-Pole signature of the notched elliptical dipole tag with the highest frequency notch removed.

The pole at 3.1 GHz that was conjectured to be attributable to the base dipole structure is again present further strengthening this assumption. While the location is not exactly the same, it is very close only differing in frequency by 0.004 GHz. The magnitude of the residue as indicated by the color bar is also similar, especially when considered relative to the other poles. This again suggests it is the same pole as observed for the previous two cases.

3.5.3 Highest and Lowest Present

In this permutation, the middle frequency notch is removed, leaving the highest and lowest frequency notches (binary 101). Looking at the frequency domain form of the scattered fields in Figure 3.15 shows that there are now only two nulls present. The lowest frequency null appears consistent with the ideal case, however the null that should be attributable to the highest frequency notch has shifted 1.4 GHz lower in frequency to 8.1 GHz. This indicates that the middle and high frequency notches are strongly coupled behaviorally.

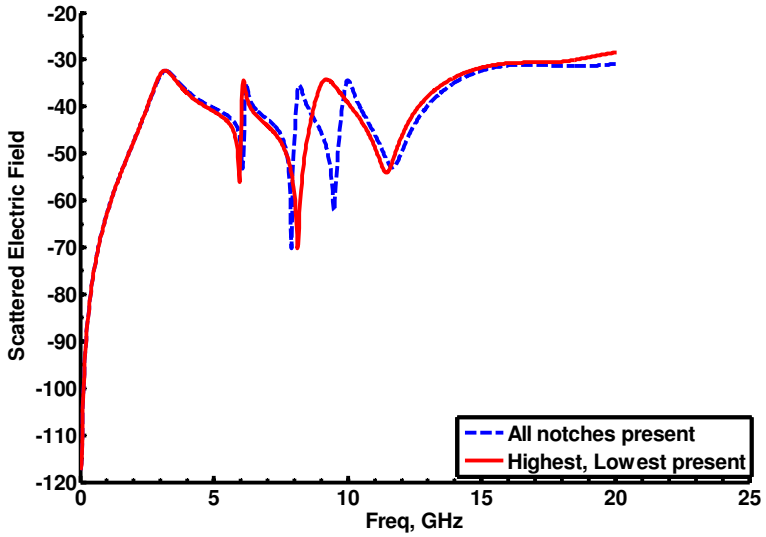

Figure 3.15-Simulated Scattered Electric Fields of the notched elliptical dipole tag with the middle frequency notch removed.

Looking at the pole signature of Figure 3.16 reveals that the middle frequency pole at 8.1 GHz is now absent. This indicates that the pole 8.1 GHz is attributable to the middle frequency notch. The pole at 3.1 GHz is again present and has a residue magnitude consistent with all previous cases further strengthening its connection to the base dipole structure. As expected from the frequency domain response, the pole due to the highest frequency notch is shifted down in frequency moving from 9.9 GHz to 9.1 GHz.

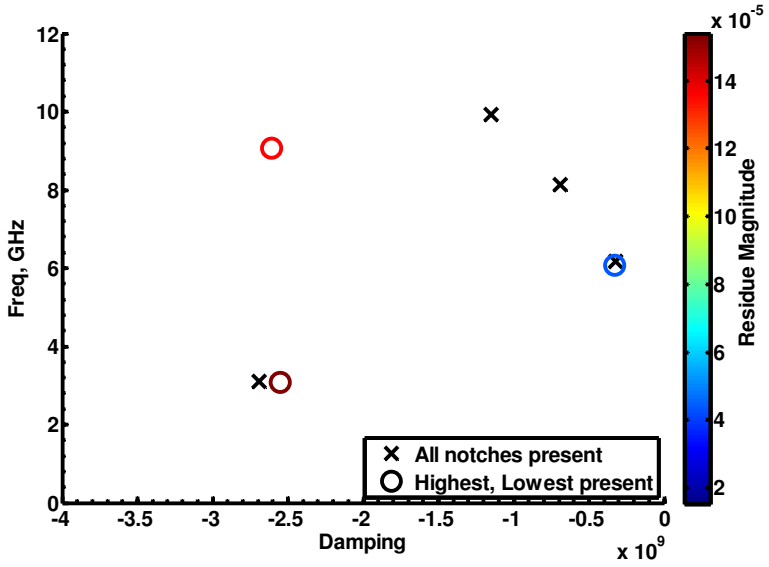

Figure 3.16-Pole signature of the notched elliptical dipole tag with the middle frequency notch removed.

Perhaps more interesting is the dramatic increase in damping of the high frequency notch's pole. Licul in his work using pole singularities to characterize antennas suggests an explanation for this increase in damping. Narrowband resonant structures are characterized by poles with less damping, and conversely wideband structures are characterized by less damped poles [20]. Removing an adjacent notch creates a less restrictive current path around the remaining notch thus making it a less narrowband structure and increasing the damping of associated poles. If the currents are not tightly bound to the notch, the effective length would also be longer accounting for the shift lower in frequency.

3.5.4 Highest and Middle Present

For this permutation, the lowest frequency notch has been removed from the structure, leaving the highest and middle notches (binary 110). Considering the frequency domain response in Figure 3.17 reveals that by removing the lowest frequency notch, the lowest frequency null originally present in the ideal response is now absent. The middle frequency null has been shifted down in frequency moving from 7.9 GHz to 6.6 GHz indicating that the behavior of the middle notch is coupled to the lowest frequency notch. The highest frequency null is shifted slightly down in frequency moving from 9.5 GHz to 9.4GHz. This indicates that the highest frequency null acts relatively independently from the lowest frequency notch. This relative behavioral independence can most likely be attributed to the fact that they are not located physically adjacent to each other.

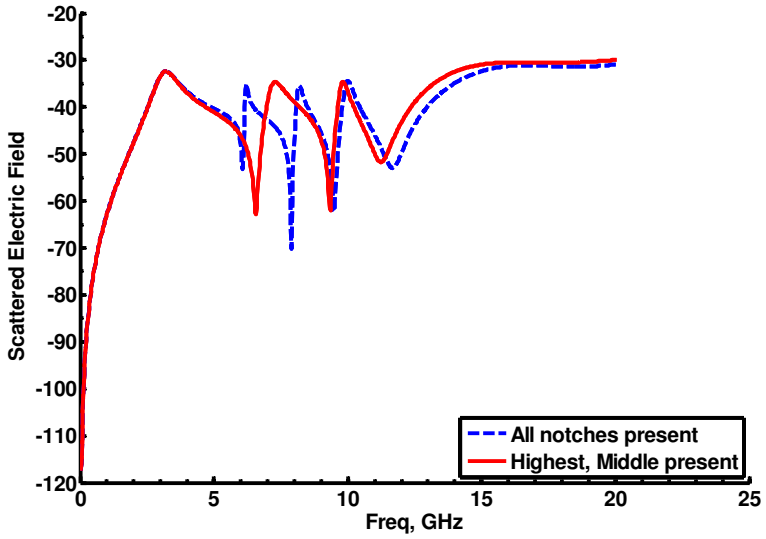

Figure 3.17-Simulated Scattered Electric Fields of the notched elliptical dipole tag with the lowest frequency notch removed.

The effects observed in the frequency domain response of Figure 3.17 translate directly into our pole signature shown in Figure 3.18. The lowest frequency pole we assumed was due to the lowest frequency notch is now absent lending credence to this assumption. The highest frequency pole remains close to the location observed for the ideal response indicating its behavior is relatively independent of the lowest frequency

notch. The middle frequency pole has shifted lower in frequency from 8.1 GHz to 7.1 GHz and higher in damping. This is in agreement with our assertion made for the previous case that removing an adjacent notch has the effect of making a notch a more wide-band structure and increasing its effective length.

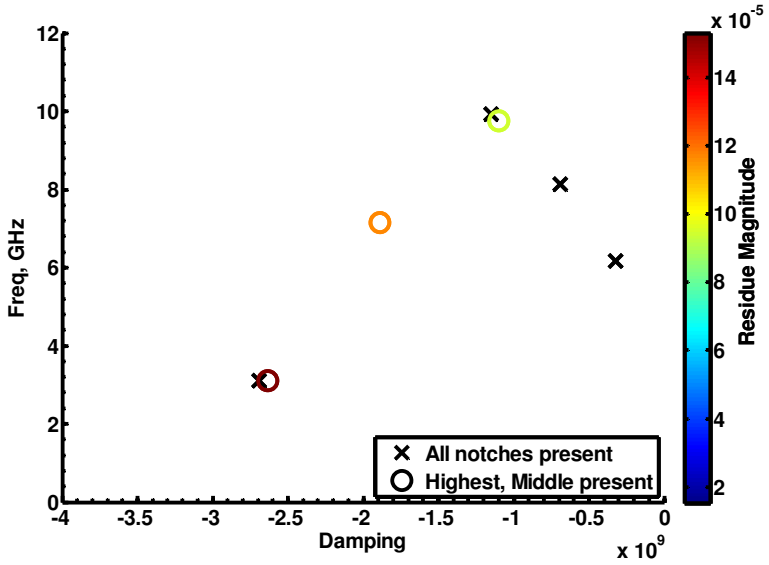

Figure 3.18-Pole signature of the notched elliptical dipole tag with the lowest frequency notch removed.

3.5.5 Highest Present

This permutation considers the case where both the middle and lower frequency notches have been removed leaving only the highest frequency notch (binary 100). Looking at the frequency domain form of the scattered fields in Figure 3.19, as would be expected two of the three nulls are now missing. The remaining null that is attributable to the highest frequency notch is shifted down in frequency. In the previous permutation with only the lowest frequency notch removed, the high frequency notch was for the most part unaffected. This combined with our current observations suggests that the highest frequency notch's behavior is strongly linked to the presence of the middle frequency notch. In this case the middle and low frequency notch are both removed and the highest frequency notch's null is shifted even lower than the case where only the middle frequency notch is removed. The middle frequency notch when present serves to separate

the low and high frequency notches behaviorally causing the lowest frequency notch's presence or absence has less of an impact on the currents surrounding the highest frequency notch. In short, for this case, we can see the effect of removing the lowest frequency notch because of the absence of the middle frequency notch.

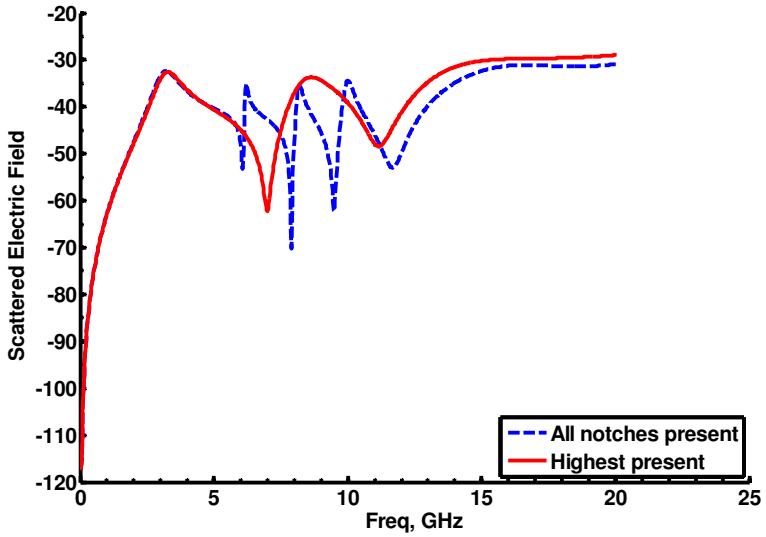

Figure 3.19-Simulated Scattered Electric Fields of the notched elliptical dipole tag with the middle and low frequency notch removed.

The changes noted in the frequency domain translate directly to the complex frequency plane. Two of the four poles present in the ideal case are now missing. The pole belonging to the base elliptical dipole structure is again present at 3.2 GHz. There is also a pole attributable to the highest frequency notch at 8.3 GHz, and as was anticipated from the frequency domain response the frequency is lower. The pole is also higher damped even more so than it was for the case with only the middle notch removed. This indicates that the lowest frequency notch is linked to the behavior of the highest frequency notch just not to the same extent that the middle frequency notch.

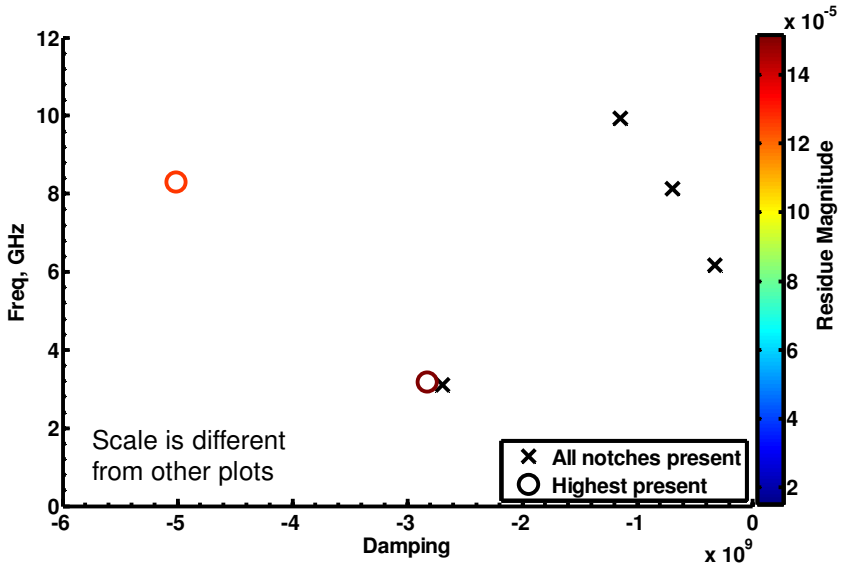

Figure 3.20-Pole signature of the notched elliptical dipole tag with the middle and lowest frequency notches removed.

3.5.6 Middle Present

For this permutation, the lowest and highest frequency notches have been removed leaving only the middle frequency notch (binary 010). This is evident in the frequency domain scattered fields of Figure 3.21 as instead of three distinct nulls we now only have one null located at 6.6 GHz. By process of elimination, this is the null resulting from the presence of the middle notch. For the ideal case the middle notch null was located 7.9 GHz. It has obviously been shifted lower in frequency due to the removal of the highest and lowest frequency notches.

Looking at the pole signature in Figure 3.22 reveals that we now only two poles. We have removed two sources of poles, and two poles have been removed from the signature. The pole that we have previously indicated as being inherent to the dipole structure is again present near 3.1 GHz. Another pole is present at 7.1 GHz and presumably due to the middle notch. With all notches present, the middle notch creates a pole at 8.1 GHz. Removal of both adjacent notches appears to have shifted the pole created by the middle notch down by 1 GHz. Similar to the previous case of only having

the highest notch present, the damping is also increased. Again, while the null is present and well defined though shifted, the subsequent peak is not as sharp.

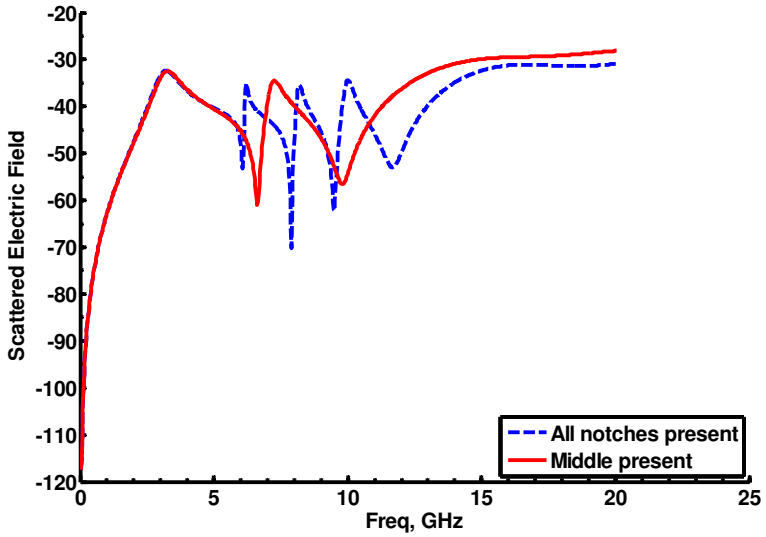

Figure 3.21-Simulated Scattered Electric Fields of the notched elliptical dipole tag with the high and low frequency notches removed.

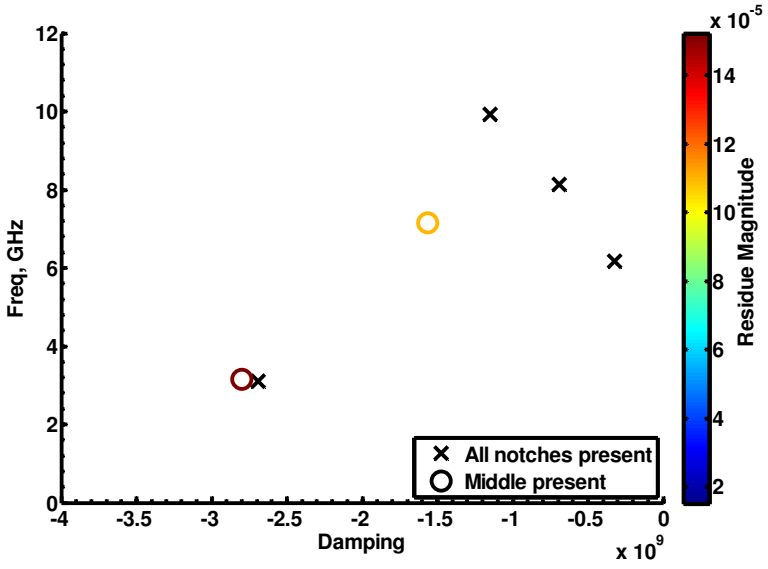

Figure 3.22-Pole signature of the notched elliptical dipole tag with the highest and lowest frequency notches removed.

3.5.7 Lowest Present

In this permutation, both the high and middle frequency notches have been removed such that only the lowest frequency notch remains (binary 001). Looking at the frequency domain scattered response in Figure 3.23 shows that the two higher frequency nulls are now absent. The lowest frequency null at 6.1 GHz remains, being shifted only slightly in frequency. This suggests that the lowest frequency notch behaves for the most part independently of the other notches.

Looking at the pole signature of Figure 3.24 shows verifies that the lowest frequency pole attributable to the lowest frequency notch is present and in approximately the same location as observed for the other permutations when it was present. This indicates that the lowest frequency notch's pole is relatively invariant to the presence or absence of the other two notches. We again have the dipole structure's pole at 3.1 GHz.

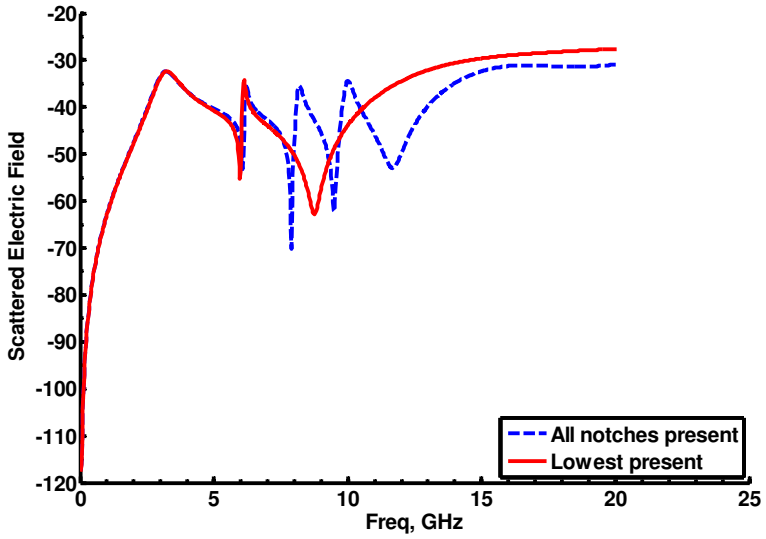

Figure 3.23-Simulated Scattered Electric Fields of the notched elliptical dipole tag with the high and middle frequency notches removed.

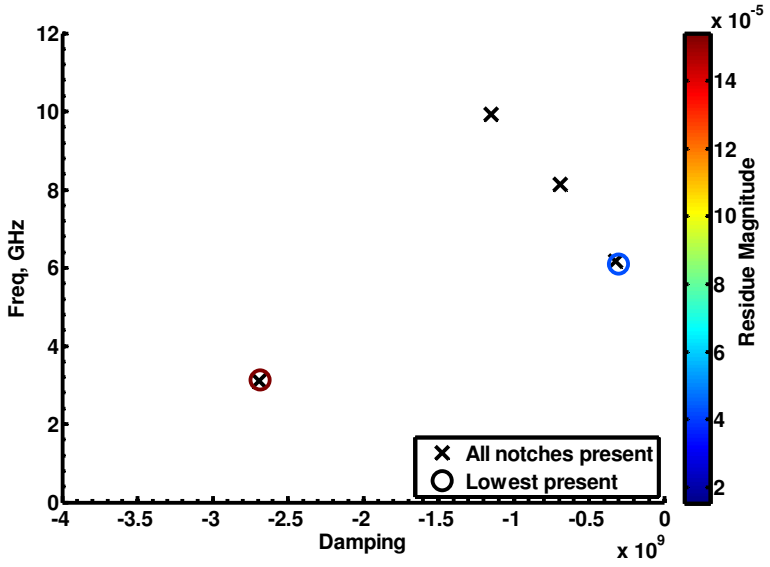

Figure 3.24-Pole signature of the notched elliptical dipole tag with the highest and middle frequency notch removed.

3.5.8 Are the poles due to the notches?

In the following, we will review the reasons we considered all these tag permutations, and how they were addressed. Recall that the justifications for considering all permutations of the tag involving notches were: verifying the poles are attributable to a specific structure in the tag, analyzing the behavior of the tag itself, and to gain insight into the practicality of encoding data using singularities.

First, we did in fact verify that the poles are attributable to specific parts of the notched dipole structure. This was one of the main purposes of considering permutations of the tag and is a critical conclusion lending support to an embedded singularity tag as it implies we have some control over if and where pole singularities exist. We were able to verify that the pole at 3.1 GHz is due to the base structure, and as would be expected was observed for all permutations. Each of the remaining three poles were attributable to their corresponding physical notch in terms of relative frequency (the highest frequency pole is due to the shortest notch, et cetera). Removing a particular notch always resulted in the disappearance of its corresponding pole on the complex frequency plane. However, it was quickly evident that the notches did not act independently of each other. In the case

where an adjacent lower frequency notch was removed, the next higher frequency notch was shifted towards a lower frequency and greater in damping. This is most likely attributable to the behavior of the currents surrounding the notches on the structure. By removing an adjacent notch, the current path surrounding the notch is less restrictive thus making it a more wideband structure and increasing the effective length.

What actually creates a pole?

Manteghi and Rahmat-Samii regarded the nulls in the frequency domain scattered fields as the feature of interest. We have continued this trend noting the behavior of the nulls, and predicting the creation of corresponding poles. However, the frequency of the resulting poles never correspond exactly to the null, but instead are always somewhat higher in frequency. Whenever we have observed a relatively low damped pole, the frequency domain response consisted of a sharp null immediately followed by a sharp peak. For all the cases where we removed a notch, and then observed a highly damped pole, the null remained relatively sharp, and the subsequent peak was broadened and less defined. This suggests that the features in the frequency domain that creates a pole and determine its frequency and damping behavior are the combination of a null and a peak in close proximity. This is also in line with our observations regarding narrowband versus wideband regarding damping of poles as a sharp feature represent a narrowband case and a broad feature a wideband case. We will continue to note the presence of nulls as an indicator of a pole, but not to say that it alone creates the pole. Future investigations could address the exact process of creating a single pole in terms of both frequency and damping.

Can we distinguish one permutation from another?

In terms of the ultimate practicality of considering each pole signature as a way to read the encoded bits, we have in fact verified it is possible. To rephrase this; can we discern different signatures for each combination of notches and thus retrieve the bits? The answer is “probably”. In this thesis, we are not going so far as to develop a decoding

algorithm and actually building a reader that simply outputs the bits of interest. We must rely on a visual inspection of the results as plotted on the complex frequency plain.

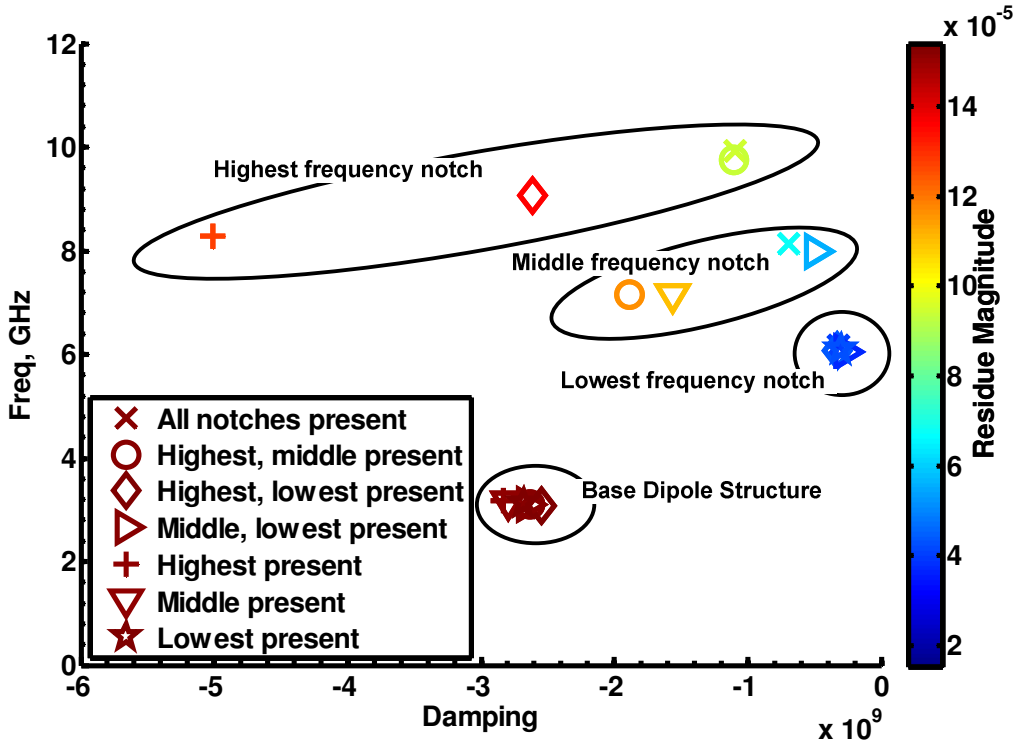

Figure 3.25-Poles for all permutations of the notched elliptical dipole tag involving removing notches.

In Figure 3.25, we have defined regions that group all poles that have been determined to be due to a particular notch. When considering the permutations one at a time, one might look at individual results and think that the poles change too much to be a reliable means for encoding and decoding information based on pole location. Specifically, the highest frequency notch pole and the middle frequency notch pole shift lower in frequency and higher in damping when the adjacent lower frequency notch is removed. However, if we consider the results in their entirety as shown in Figure 3.25, it becomes apparent that even with shifts in pole location, the poles attributable to a particular notch remain within regions that are easily separable from other notches and their poles. This suggests a possible decoding algorithm. If a pole falls inside a defined

region in the complex frequency plane, then it indicates the presence of a particular notch, and thus an appropriate 1 in the binary sequence. If no poles are observed within a region, we have a 0. In reality, pole singularities provide more data than simply frequency and damping. An encoding algorithm based on regions could be further enhanced by considering the strength of the pole (magnitude of the residue) especially when taken in context with other observed poles. We have completely ignored the phase of the poles, but this too could be of some utility.

3.6 What happens if we deviate from the ideal case?

In this section, we will consider two cases of excitation and observation that deviate from the ideal case. They could both be described as a bistatic radar scenario. For both variations considered, the tag was modeled with all three notches present and in free space.

These scenarios are for the most part intended to show the aspect independent nature of an SEM based encoding using embedded singularities. In theory, the same poles should be extracted for these scenarios as for all previous scenarios. By the "same" poles, we mean poles that have the same location on the complex frequency plane (frequency and damping). The residues are not observation or excitation independent. The magnitude and phase of the poles are subject to change. With changes in excitation and observation, it is possible that a particular pole may not be excited strongly enough to be observed. For the simulations results, not observing a pole due to strength of observation is much less likely as noise is not present. The converse is also possible. A pole that was otherwise not observed due to being sorted out, may become evident.

3.6.1 Ideal Excitation, Non-Ideal Observation

The first case considers an ideally excited tag, $\theta_{exc} = 0°$, $\varphi_{exc} = 90°$, $\eta = 90°$, but with a non-ideal observation point, $\theta_{obs} = 45°$, $\varphi_{obs} = 45°$, and $r = 1\ m$. This case is intended to show that the poles are observation position independent.

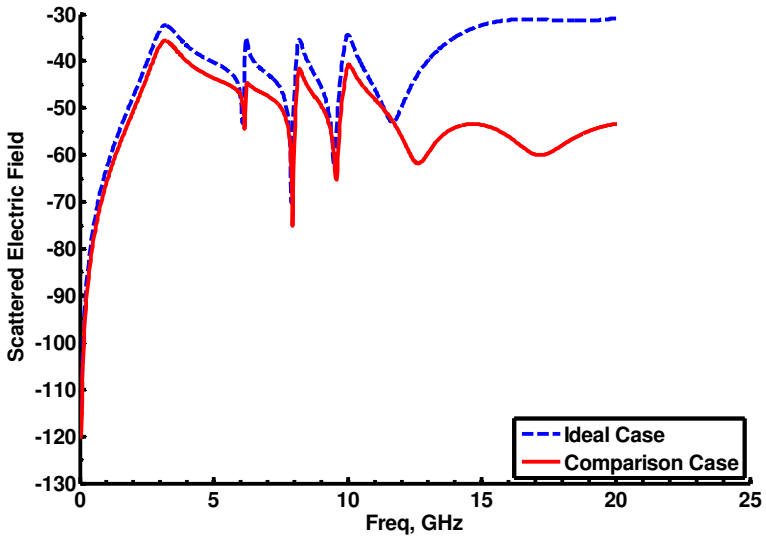

Figure 3.26-Simulated Frequency domain scattered response of the notched elliptical dipole tag for the case of $\theta_{exc} = 0°$, $\varphi_{exc} = 0°$, $\eta = 90°$, $\theta_{obs} = 45°$, $\varphi_{obs} = 45°$, and $r = 1\ m$.

The frequency domain form of the scattered electric fields, as seen in

Figure 3.26, reveal that all peaks and nulls noted in the ideal case's response are still present and are readily distinguishable visually. The magnitude of the response is diminished because the tag does not scatter equally in all directions. This scenario considers an observation point that could be described as off bore sight for the tag. This reduction becomes even more evident at higher frequencies above 12 GHz. The similarity in the frequency domain to the ideal case suggests that we should observe similar poles for this aspect variation.

Looking at pole signature in Figure 3.27, we see that we still have a pole signature that closely resembles the ideal case with the exception that the highest frequency notch has an extra pole associated with it. We could simply stop at this point and say the tag has been successfully read, as there is a nearly identical pole for each pole in our ideal case signature. However, the seemingly spurious pole warrants some further consideration.

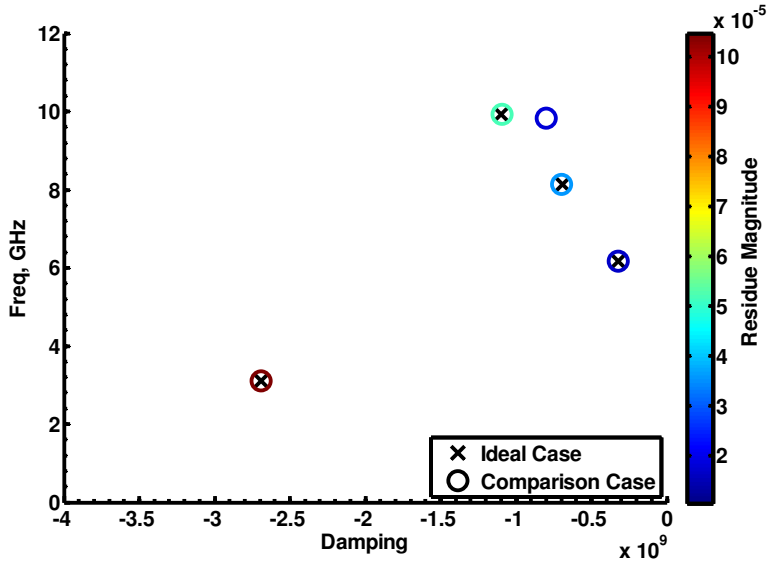

Figure 3.27-Extracted poles for the simulated scattering response of the notched elliptical dipole tag for the case of $\theta_{exc} = 0°$, $\varphi_{exc} = 0°$, $\eta = 90°$, $\theta_{obs} = 45°$, $\varphi_{obs} = 45°$, and $r = 1\ m$

In the previous results, we have mostly ignored the phase aspect of a pole representation. However, now due to a non-ideal observation point, we can observe phase differences between different sections of the tag. Looking at the tag structure in Figure 3.1, note that each notch is duplicated four times. Duplicate notches are located far enough apart spatially on the structure such as to act independently of each other and thus should each have their own poles independent of the other notches. When considering the ideal case we only observed a single distinct pole for each notch size. What we were really observing are four poles that are in phase and equally excited. The ideal case is such that that all quadrants of the tag are symmetrical in terms of excitation and observation. The effect of having several poles that are otherwise identical but with different phases would change the magnitude of the residue of the single pole they could be interpreted as. Therefore phase should not account for the extra pole. We must assume that something else accounts for the multiple pole extraction.

A better explanation for this pole is that it is in fact a natural pole of the structure that we did not observe for the ideal case. In fact, if we vary the time window, the extraneous pole is consistently extracted along with the expected poles of the ideal case

signature. This indicates that it is perhaps not spurious, but a natural oscillation. Anything spurious in nature should not be consistently extracted. Due to the frequency location, this new pole is most likely due to the presence of the highest frequency notch. This suggests that perhaps forming a signature to use for reading a tag should not be based on only a single aspect.

It is also possible the extra pole is a curve fit pole extracted by the Matrix pencil algorithm. The signal is perhaps too complex to be represented by a single pole. The next section and variation explores this explanation.

3.6.2 Non Ideal Excitation, Non-Ideal Observation

The second cases considers a non-ideal excitation in the sense that it is not normally incident and not polarized solely in the $\hat{x}$ direction. In terms of our coordinate system, this is $\theta_{exc} = 45°$, $\varphi_{exc} = 225°$, $\eta = 90$ °. The observation point is also located non-ideally as it is not collocated with the excitation source. In terms of our coordinate system, this is $\theta_{obs} = 45°$, $\varphi_{obs} = 45°$, and $r = 1\ m$.

The resulting frequency domain scattered fields, as shown in

Figure 3.28, reveal that we do not have distinctly defined nulls as we have had for all the previous cases. This is perhaps the first scenario where we cannot immediately make the assertion that the notches are present based on the frequency domain scattering response and that the resulting pole signature should resemble the ideal case based on the frequency domain response. This inability to interpret the frequency domain hints that we may see one of the suggested advantages of a pole signature: discrete points as the metric of interest. Rather than trying to read into the frequency domain response, we will move on to considering the poles.

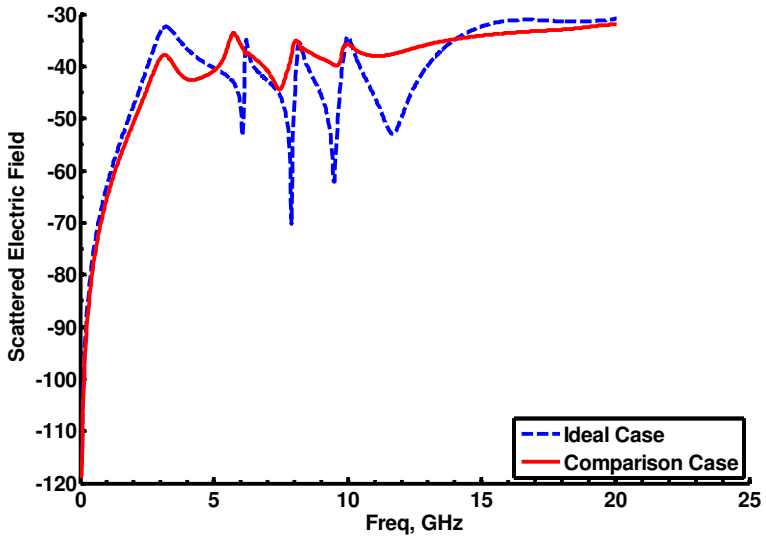

Figure 3.28-Simulated Frequency domain scattered response of the notched elliptical dipole tag for the case of $\theta_{exc} = 45°$, $\varphi_{exc} = 225°$, $\eta = 90°$, $\theta_{obs} = 45°$, $\varphi_{obs} = 45°$, and $r = 1\ m$.

If we again use the suggested region based decoding algorithm suggested at the end of the permutation section, the poles in Figure 3.29 indicate that pole signature can be successfully read. For each of the poles in the ideal case signature, we have at least one pole extracted that is nearby. For the middle and high frequency notches, we now have multiple poles of similar frequency but of variable damping. We could simply say the tag is readable and move on. However, we will first consider a few things.

Are we seeing natural oscillations not previously observed?

Just like our immediately previous scenario, there are poles present that were not present for the ideal case. The poles located at 5.70 GHz and -1.28E9 damping, 5.75 GHz and -3.485E9 damping, 7.65 GHz and -2.64E9 damping have not been previously observed and thus warrant some extra attention. Altering the time windowing has little effect on its location and strength. This invariance could be considered an indicator that the poles do in fact exist. Saying that a poles does in fact "exist" is to imply it is a natural oscillation of the structure and not simply a curve fit pole. A study combining structural permutations with different forms of observation and excitation could lead to the

conclusion that these poles are natural oscillations. Similar to our observations in the previous case, forming a tag signature for the purpose of reading should involve considering permutations in conjunction with different excitations and observation points.

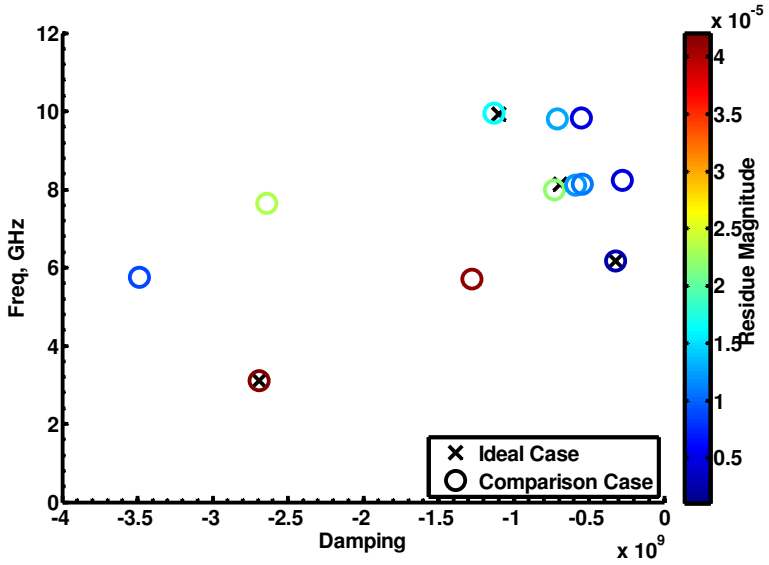

Figure 3.29-Poles extracted from the simulated tag response with $\theta_{exc} = 45°$, $\varphi_{exc} = 225°, \eta = 90\ °, \theta_{obs} = 45°, \varphi_{obs} = 45°$, and $r = 1\ m$.

Can we use the SVD sorting feature to reduce the number of poles?

It might be tempting to use the SVD sorting feature to eliminate what one would call "spurious" poles simply because they were not observed for the ideal case which forms our pole signature. They are not spurious in the sense that they are caused by noise as we are considering noiseless simulations. However, it is possible that the Matrix pencil algorithm generates spurious poles due to an inability to correctly interpret a more complex signal resulting from multiple poles of identical or similar frequencies.

Looking at the groups of multiple poles in Figure 3.29 surrounding the ideal case pole for the high and middle frequency notch, notice that for both groups there is one pole that is stronger than all others. This suggests that perhaps a single pole could represent the whole group.

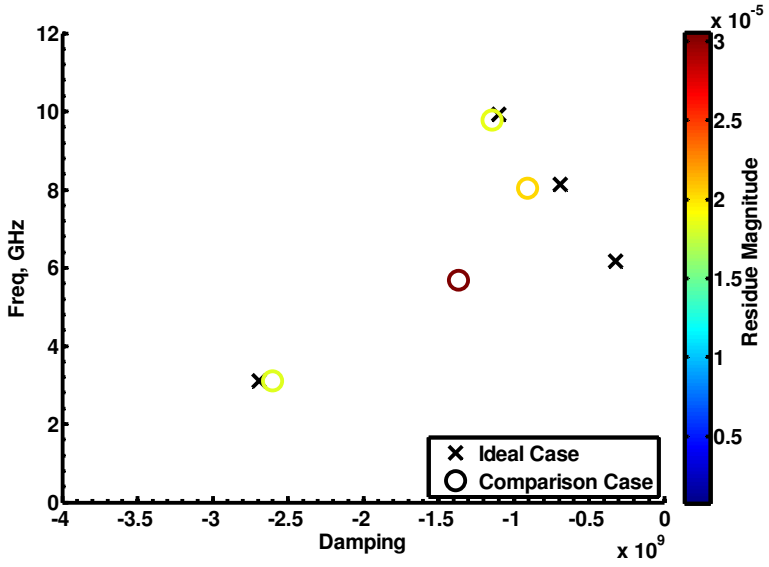

Figure 3.30-Poles extracted from the simulated tag response with SVD sorting parameter p = 2. $\theta_{exc} = 45°$, $\varphi_{exc} = 225°$, $\eta = 90\ °$, $\theta_{obs} = 45°$, $\varphi_{obs} = 45°$, and $r = 1\ m$.

If we reduce the SVD sorting parameter to p = 2, we reduce the multiple poles to a single stronger pole and get the pole signature of Figure 3.30. We now have a single pole for both the high and middle frequency notches. However, we no longer have a pole for the lowest frequency notch. In Figure 3.31, comparing the reconstructed time-domain wave-form for the reduced pole signature to the direct from simulation wave-form shows that the reduced pole signature still models the original waveform and also matches the non-reduced pole signal.

The low frequency notch pole is the least damped of the poles. If we consider a time window that is later in time such that the higher damped poles have decayed, it is possible it will not eliminated by the SVD sorting. This is in fact the case if we use the time window of Figure 3.33. The pole signature extracted using the lowered SVD threshold and the later time window results in the pole signature of Figure 3.32 which now includes a pole attributable to the low frequency notch.

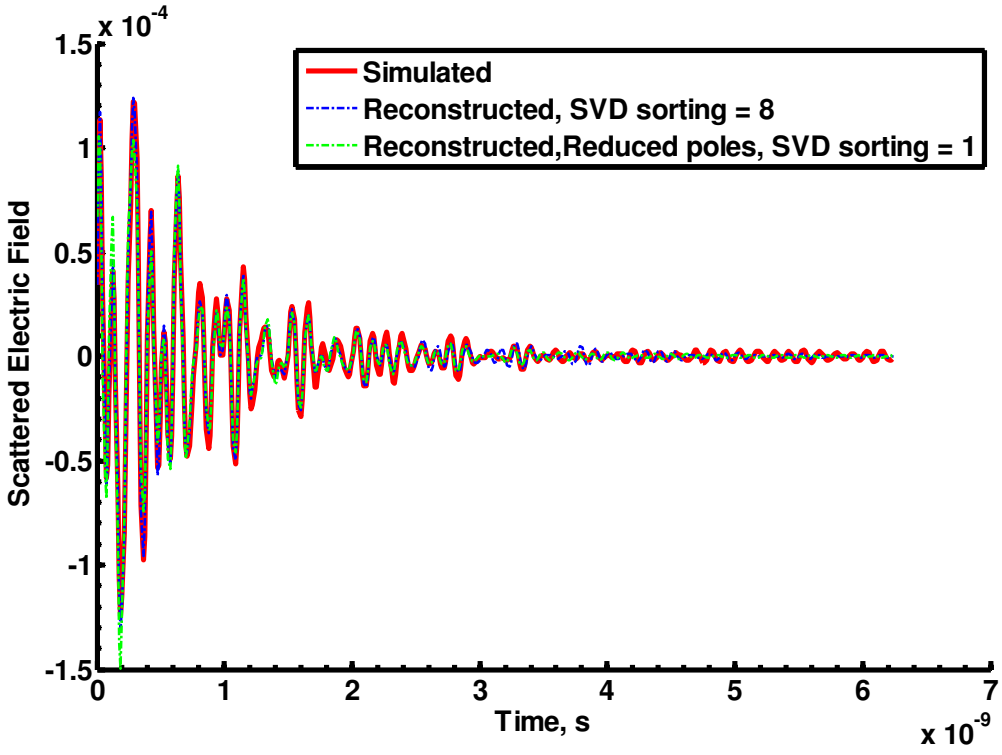

Figure 3.31-Comparison of original time domain versus that reconstructed from poles for the simulated scattered response with $\theta_{exc} = 45°$, $\varphi_{exc} = 225°$, $\eta = 90\ °$, $\theta_{obs} = 45°$, $\varphi_{obs} = 45°$, and $r = 1\ m$.

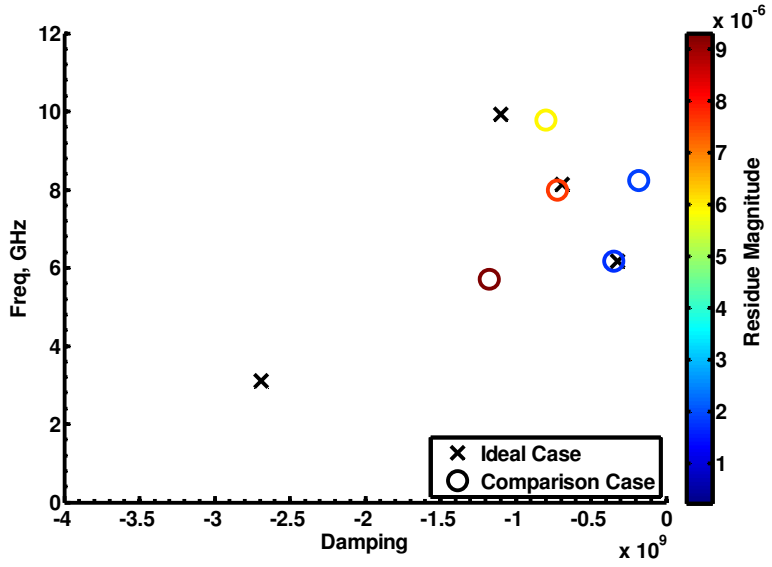

Figure 3.32-Poles extracted from the simulated tag response with SVD sorting parameter p = 2 and a later time window. $\theta_{exc} = 45°$, $\varphi_{exc} = 225°$, $\eta = 90°$, $\theta_{obs} = 45°$, $\varphi_{obs} = 45°$, and $r = 1\ m$.

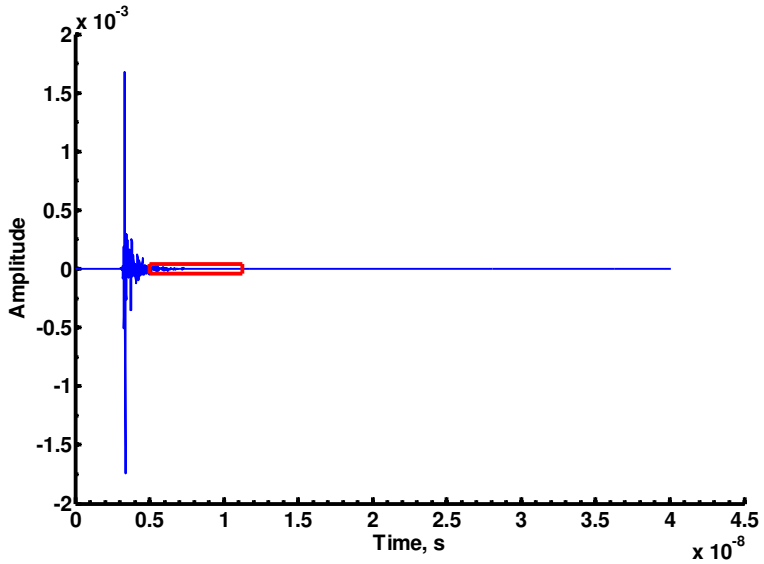

Figure 3.33-Later time window used to observe the low frequency pole.

Another explanation for the pole groupings

If we take the grouping of poles that would be attributable to the middle notch based simply on proximity to the ideal case pole, and look at what they represent in the

time domain, we get the signal in Figure 3.34. This signal appears to have a ringing element present. It is not simply a decaying sinusoid. The poles that form this grouping have frequencies of 8.00, 8.11, 8.16, 8.23 GHz going from least damped to most damped. Note that they consist of a serious of poles close in frequency, but no two identical. Also note that the 8.00 GHz is excited stronger than the remaining three. The poles account for the ringing by having the 8.0 GHz pole form the bulk of the signal and having the remaining weaker poles drift in and out of phase with the main pole. The less damped poles account for the ringing later on in the signal. This ringing explanation for the pole groupings becomes more plausible as there is a physical explanation for the ringing. Energy can be coupled to other portions of the tag, and then later in the response excite a notch

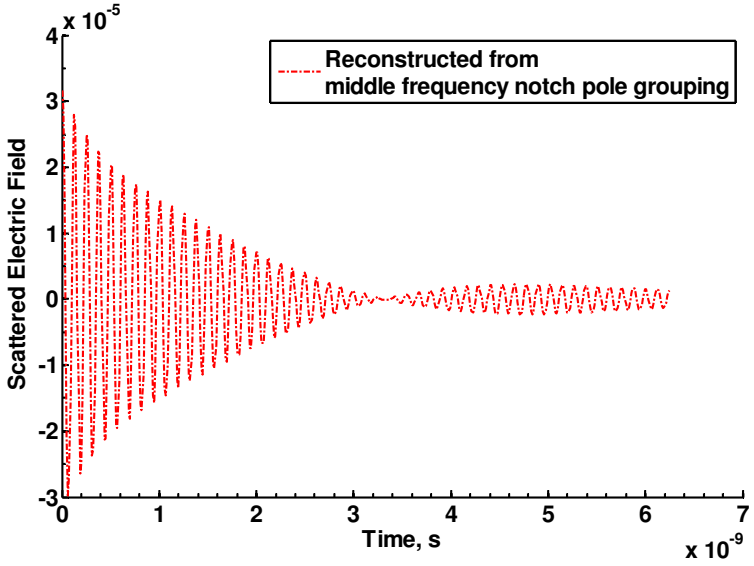

Figure 3.34-Signal represented by the grouping of poles around the middle frequency notch ideal case pole in Figure 3.29.

Are the poles aspect independent?

The aspect independent nature was observed for both cases in that with a little work we were able to extract poles corresponding to our pole signature. While we cannot say that the results were perfect in the sense that we were always able to extract exactly the same poles, it was often explainable by the fact that the initial ideal case results were

misinterpreted regarding as to what poles were actually present. For some cases with changes in excitation and or observation we did find poles exactly matching the ideal case signature which does indicate an aspect independent nature. It is also clear that the behavior of the tag is more complex than that suggested by the four poles of the ideal case. Poles that were previously not observed, become apparent with changes in observations and excitation. While it would certainly be interesting to account for each and every pole observed and be able to attribute them to physical features on the tag, we will settle for being content with having extracted the pole signature and successfully read the tag for both non-ideal cases considered. Additionally, the Matrix pencil algorithm is not guaranteed to extract the true poles of the structure. This is always a concern. Are we seeing natural oscillations of the structure, or are we see seeing a curve fit?

3.7 Monostatic Radar, A Possible Reader Configuration

In this section, we will consider cases that mimic a monostatic radar setup. This is the configuration used to take measurements, and some of the cases considered in this section were measured. The ideal case falls into this category, and is used as the basis of comparison. Due to the limited effects of the dielectric substrate on the tag behavior, the dielectric was omitted from the simulation despite the fact that these simulations are intended for a direct comparison to measured results. When comparing simulations against measurements, we will simply expect a slight frequency shift.

Rather than considering an exhaustive number of possible orientations, these scenarios consider the extremes of possible tag orientations. We will continue to use our coordinate system as defined in Figure 3.3 to define the scenarios being considered. However, when describing them, a viewpoint from that of the observer will be used. By observer, we mean what one would see if looking at the tag from the point at which the measurement antennas are located looking directly at the tag. From an observer view point, we will consider the tag as either oriented “normal”, that is with the $\hat{z}$ vector pointed at the observer, or with the tag oriented rotated 90° about either the x or y axis such that the $\hat{z}$ is orthogonal to the vector defining bore sight of the horn antennas . We

will term the rotated case as "on edge". The next two extremes are regarding the polarization of the incident fields. We will consider the case of the electric field being $\hat{x}$ polarized, which we will refer to as co-polarized, and also the case of the electric field being $\hat{y}$ polarized which we will refer to as being cross-polarized.

Combining the two types of extremes yields four possible combinations; normal co-polarized, normal cross-polarized, on edge co-polarized, and on edge cross-polarized. The ideal case is the normal co-polarized case, which has already been analyzed. It will not be presented as a separate case, but instead will continue to be used throughout as a comparison for the other cases.

3.7.1 On edge Co-Polarized, $\boldsymbol{\theta_{exc} = \theta_{obs} = 90°}$, $\boldsymbol{\varphi_{exc} = \varphi_{obs} = 90°}$, $\boldsymbol{\eta = 90°}$, and $\boldsymbol{r = 1\ m}$.

The first case considers the tag flipped on edge. While this is considerably different from the ideal case, the excitation electric field is polarized correctly to excite the notches so it is not unreasonable to expect some meaningful results. In fact, the frequency domain fields of Figure 3.35 do have some similar features to that of the ideal case which suggests that we should observe some of the same poles. The null and peak for the lowest frequency notch is present, and appears to be even more defined. The middle notch null is present, but the immediately following peak is altered. The highest frequency notch's features are considerably different from the ideal case, specifically the null is absent. But the peak is still present. For each notch we still have some features in the frequency domain, so it is possible that usable poles will be observed.

Looking at the pole signature in Figure 3.36, we again see clusters of multiple poles near our ideal case signature poles for the high and middle notches. As with the cases considered in the previous section, SVD sorting could be used to reduce the occurrence of multiple poles surrounding the ideal case signature poles. However, in this case despite having clouds of multiple poles, we also have poles that nearly exactly fall on the ideal case signature pole locations. Because of this, we will not do any further work with time windowing and or SVD sorting and consider this orientation of the tag readable.

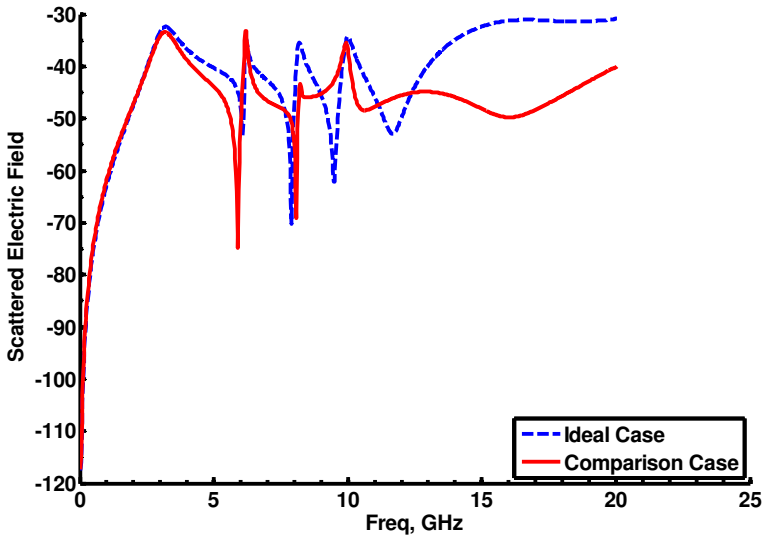

Figure 3.35-Simulated Frequency domain scattered response of the notched elliptical for the on edge co-polarized case

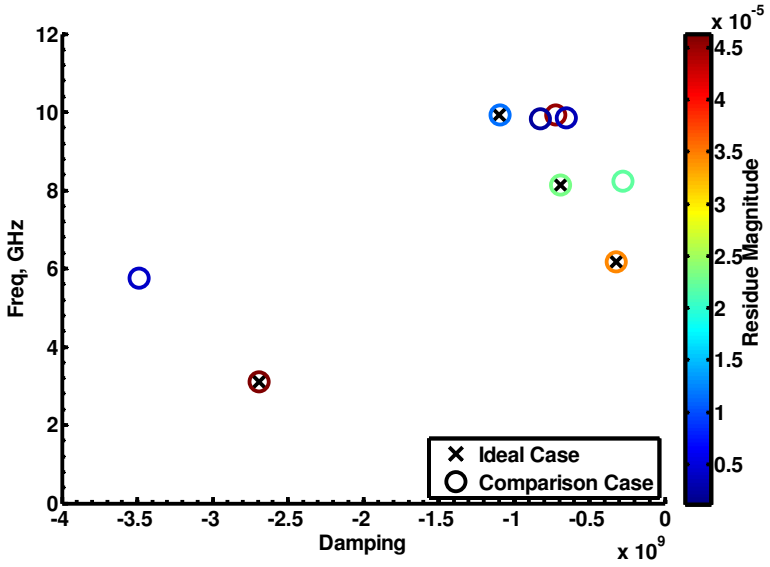

Figure 3.36-Poles extracted from the simulated tag response of the notched elliptical for the on edge co-polarized case.

.

3.7.2 Normal Cross-Polarized $\theta_{exc} = \theta_{obs} = 0°$, $\varphi_{exc} = \varphi_{obs} = 0°$, $\eta = 90°$, and $\rho = 1\ m$.

This case considers a normally oriented tag similar to the ideal case with the exception that the excitation is polarization in the $\hat{y}$ direction. This is cross-polarized relative to the ideal excitation to excite the notches, and it is not expected that the effects of the notches will be observable.

Looking at the frequency domain response in Figure 3.37 shows that due to being excited in a non-ideal manner, and thus not exciting the notches, the nulls attributable to the notches are absent. Based on the lack of observable features in the frequency domain, the pole signature is expected to deviate significantly from that of the ideal case.

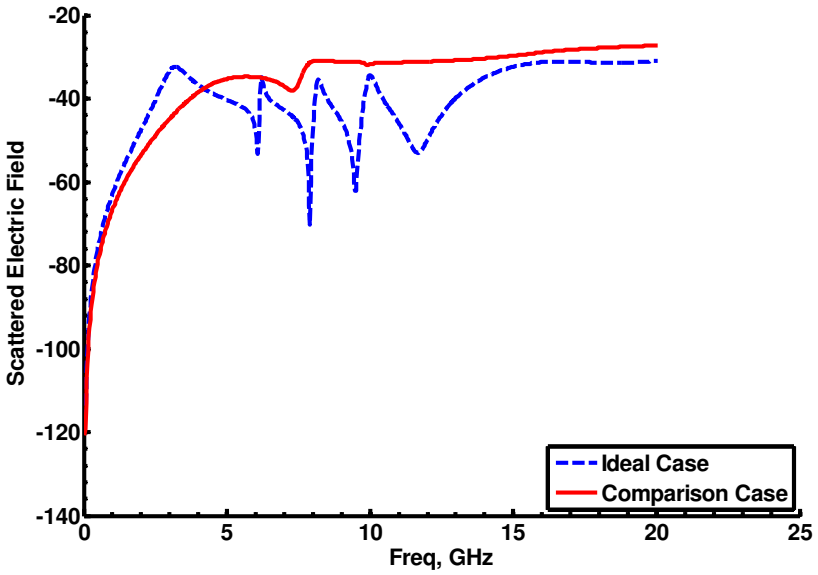

Figure 3.37-Simulated Frequency domain scattered response of the notched elliptical for the normal cross-polarized case

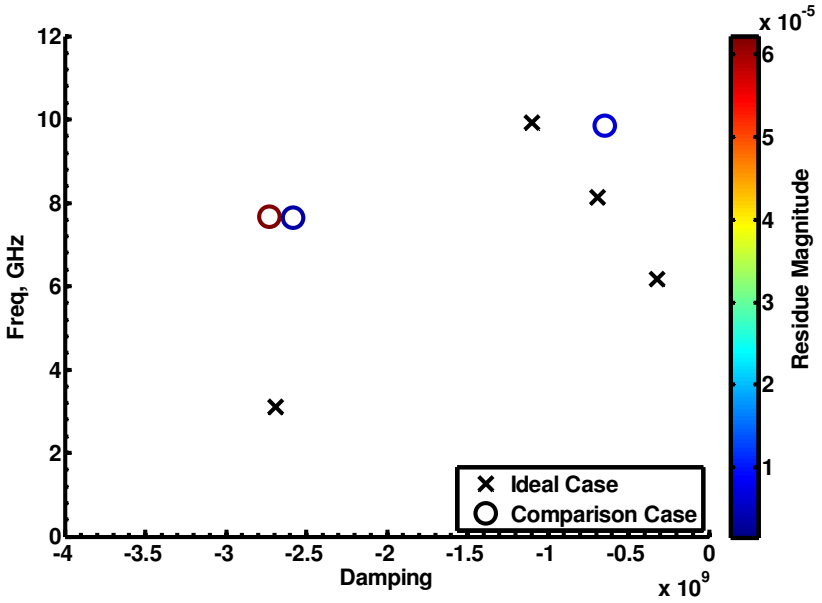

Figure 3.38-Poles extracted from the simulated tag response of the notched elliptical for the normal cross-polarized case.

3.7.3 On edge Cross-Polarized $\theta_{exc} = \theta_{obs} = 90°$, $\varphi_{exc} = \varphi_{obs} = 0°$, $\eta = 90°$, and $\rho = 1\ m$.

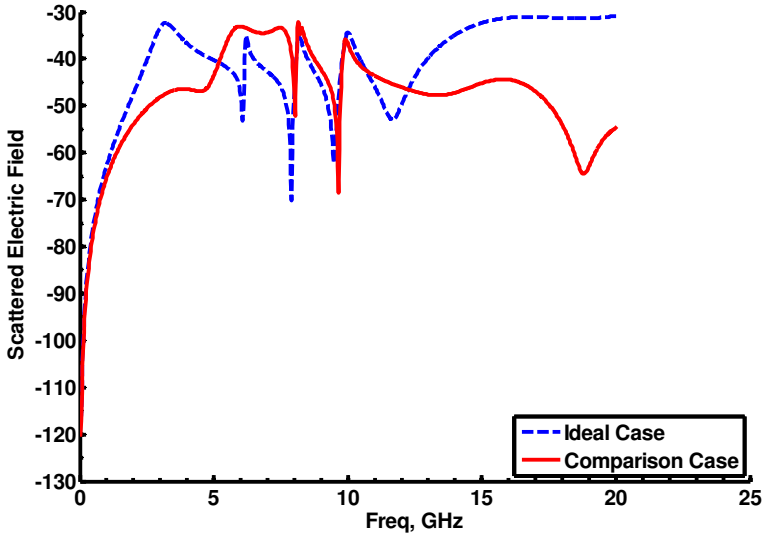

Figure 3.39-Simulated Frequency domain scattered response of the notched elliptical for the on edge cross-polarized case

As expected based on the frequency domain response, the extracted poles of Figure 3.38 reveal that this scenario differs considerably from that of the ideal tag signature. There is a pole at 9.85 GHz which suggests that the highest frequency notch was excited to some extent. However, the magnitude of the residue for this pole is small being only 0.086 in value if all residue magnitudes are normalized to the peak. It is more than likely that in a measurement environment with noise present this pole would not be observable. For this case, the tag is not predicted to be readable.

For the previous cross-polarized case with normal excitation incidence, the nulls and peaks attributable to the notches were more or less absent. This case is also technically cross-polarized, but the frequency domain scattered response of Figure 3.39 shows that two nulls are present. These nulls appear to correspond to the highest and middle frequency notches, suggesting that they were excited to some extent. The lowest frequency notch does not appear to have been excited at all.

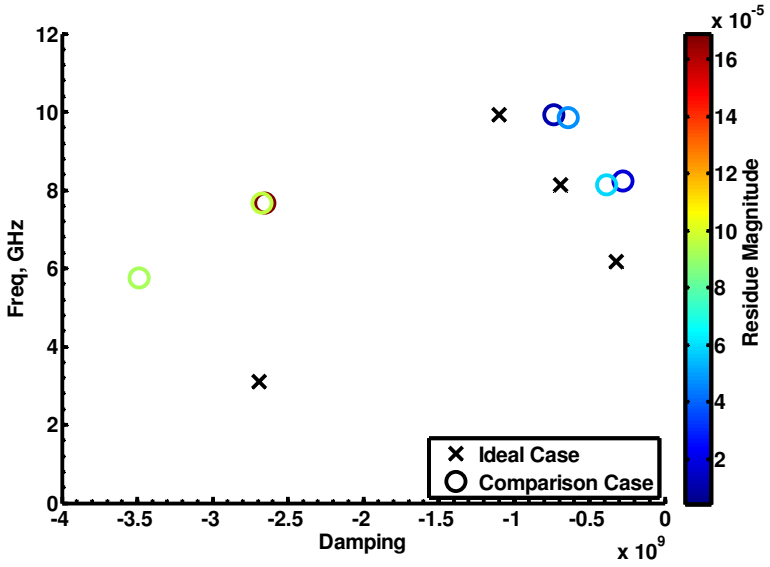

Figure 3.40-Poles extracted from the simulated tag response of the notched elliptical for the on edge cross-polarized case.

The observations made in the frequency domain do in fact translate over to the extracted poles of Figure 3.40. There are poles present with similar frequencies but higher damping corresponding to the high and middle notch ideal case signature poles. However, none of the high and middle notch poles are excited strongly. They also exhibit

higher damping than the previously observed groupings. This possibly indicates the indirect nature in which the notches were excited due to the cross-polarization. The notches are not excited directly, but rather another part of the tag is excited and then coupled to the notch. As predicted by the frequency domain response, the low frequency notch does not have a pole extracted for it. While this case is curiously more promising than the normal cross-polarized case, whether or not it could be successfully read is questionable. Recall that when the lowest frequency notch was removed, the behavior of the middle notch and its associated pole is altered dramatically. If the poles for the middle notch are not altered in the manner predicted by the absence of the lowest frequency notch, then this could interpreted as the lowest frequency notch being present despite the fact that no poles were extracted for it. However, due to the weakness with which the high and middle notch poles were excited, with noise present in an actual measurement it is quite possible they will not be observable.

3.8 Conclusions

In this chapter, the notched elliptical dipole tag's scattered fields resulting from an impulsive plane illumination were simulated and considered both in the frequency domain and also in the form of pole singularities. The single most important result of this chapter, was the establishment of a reference pole signature that will be used in the next chapter for the purposes of reading a real tag.

CHAPTER 4

Measurements, Can we read a real tag?

In the previous chapter, we were able to simulate the scattered fields due to an incident plane wave and extract a pole signature from the scattered fields. This pole signature is the perhaps the single most important result presented in this thesis as we have reached our goal of considering a tag in terms of its complex plane singularities. However, simulations represent an ideal scenario. There is no noise, you can specify arbitrary excitations, and no antennas or receivers are needed to observe the scattered fields. Simulations allow you to observe responses that one might call "pure". There are no background objects, no multipath, or any other undesired signals present.

In this section, we take the next step in considering a tag in terms of a complex plane singularity signature by measuring a real prototype tag and attempting to extract the pole signature. While these results are still not truly practical as the measurements are taken in a controlled laboratory environment, successfully reading a real prototype tag is much more indicative of the practicality of our proposed embedded singularity tag.

This section progresses as follows. First, the measurement setup will be described in detail. Next we will discuss what measurements are required and why. We will then consider how to process the data to isolate the desired tag signature by fully working through the measured results for the ideal case. Finally, we will consider the resulting measured pole signatures for a few select excitation/observation scenarios. As before, not

all of the intermediate steps for the variants are presented as there is little information to be obtained from them.

4.1 Measurement Setup

The basic measurement setup is that of a monostatic radar designed to capture the scattered response of the patch in a manner similar to that of an actual tag reader. Figure 4.1 shows the measurement arrangement consisting of two horn antennas. One antenna acts as an excitation antenna, and the other antenna receives the scattered response. For all measurements, an EM systems quad-rigid Model A6100 horn, and a DRG-118/A horn were used. The A6100 is specified to cover 2-20 GHz. The DRG-118/A is specified to cover a frequency range from 1-18 GHz.

For all discussions regarding measurements, the same coordinate as defined for the simulations in Figure 3.3 will be used. The horns remained stationary for all measurements. Conceptually the argument could be made to have the coordinate system remain fixed to the measurement setup. However, to facility direct comparison to simulated results, the coordinate system as defined remaining fixed to the tag was retained.

All measurements including the tag were taken with the tag located 1 meter away from the apertures of the horns. A scattered response from a tag or object of interest located at 1 meter has a round trip free space propagation distance of 2 meters, or the equivalent of ~6.6 ns in terms of time. As a result, the response of any objects that are being measured should appear no earlier than ~6.6 ns in the time domain. 6.6 ns is not expected to be exact as the measurement setup was not calibrated so as to have the physical aperture of the horns as the reference. The measurement was calibrated to the end of the cables. The actual onset of any desired measured response should be observed at slightly more than 6.6 ns. Responses that are extraneous are obviously excluded from this expectation (coupling, background scattering) and should be observed at times either earlier or later than 6.6 ns. While it is possible for extraneous scattering to occur at 6.6 ns, it is expected that any occurrence should be reduced in magnitude compared to other responses as they would have to result from multipath and or objects not located in the

main beam of the horn antennas. Using 6.6 ns as a reference should be sufficient to discern desired responses from undesired responses.

The two horns are collocated and co-polarized. Due to being in close proximity to each other coupling was anticipated. To reduce coupling a piece of absorbing foam was placed between them extending slightly in front of the physical apertures. The absorbing foam can be seen placed between the horns in Figure 4.1. Coupling was observed in the measurements, however no effort was made to quantify any reduction in coupling the absorbing foam may have caused. The coupling is readily observable in the time domain and can be seen in Section 4.3. This coupling was considered extraneous to the observation of the tag response. The processing techniques used to eliminate the coupling from the measurements are also detailed in this section.

All measurements were taken inside the VTAG anechoic chamber using an HP8510 to measure S_{21} of the antenna link for a frequency range of 50 MHz to 20.05 GHz with 25 MHz steps for a total of 801 points. Ideally, S_{21} would consist of fields radiated by one horn, scattered by objects, and then received by the other horn. This setup should act as a reader, recording the scattering response of a desired object when placed bore sight to the horns. This frequency range is outside the measurement range of the horns. When the horns are considered as a combined system, the range of measurements frequencies are both above and below the manufacturer specified operational frequencies. Taking the most restrictive upper and lower limits of both horns provides us with the frequency range over which the measurements are expected to be valid. The highest lower frequency range limit comes from that of the A6100 which has a lower limit of 2 GHz. The upper limit is set by the DRG-118/A, which has an upper limit of 18 GHz. Combining these two limits results in an expected valid measurement range from 2 GHz to 18 GHz. This limitation was anticipated, and acknowledged during the formulation of measurement procedures. The behavior of the tag that is of interest (notch resonant behaviors), occurs inside these limits. It was decided to proceed using the range of 50 MHz to 20.05 GHz and see if the horn response misbehaves as a matter of curiosity and perhaps as a sanity check to the validity of the measurements. The measured data

ultimately required extra processing to deal with data outside the specified frequency range of the horns.

4.2 Required Measurements

Before extracting the poles and residues, the measured data requires extra treatment due to the presence of undesired elements, specifically; the contribution of the horns, coupling between the horns, and scattering from background objects. In order to remove these undesired components, three different measurements are required. What follows is a description of each required measurement, and what the measurement is expected to contain. Each section is titled with the term that will be used to refer to a particular measurement.

4.2.1 Reference Measurement

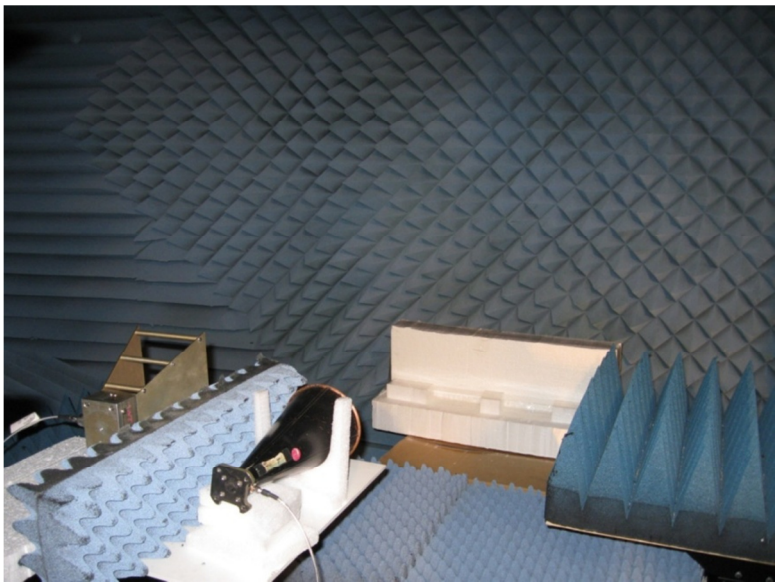

Figure 4.1-Reference Measurement

First a measurement with no objects present in the plane of measurement is needed. This measurement setup is pictured in Figure 4.1, and the co-located horns are evident on the left side of the picture. A Styrofoam bracket block can also be seen in Figure 4.1. The bracket block was constructed to enable the removal and placement of

objects consistently in the same location and is located 1 meter away from the horn physical apertures. The bracket block serves to located any objects measured in a plane of measurement 1 meter away from the horn apertures.

Being that there is no tag present this obviously does not contain the desired tag response, but rather only things that are undesired and thus need removed or processed out. Equation 4.1 reflects the expected responses that will be recorded in this measurement.

$$s_{12a} = Coupling(H_1, H_2) + Background\ Scattering \qquad \textbf{Equation 4.1}$$

The coupling is due to the horns being in close proximity to each other. When observing the coupling between the horns as a time domain response, the bulk of the coupling should occur earlier in time than any other responses and be immediately discernable when looking at a plot of the time domain response. Conversely, the background scattering is expected to be attributable to objects that are further in distance from the horn physical apertures than the point where an object being measured would be located. As a result, any responses due to scattering from background objects should occur later in time than any of the other expected responses and again be readily discernable in the time domain form of the measured response. The exact nature and location of the background scattering objects are unknown and no attempts were made to characterize them. The result is that the observed onset in the time domain of any responses attributable to background scattering are simply left as being "late time" and ultimately removed.

4.2.2 Ground Plane Measurement

The second measurement requires placing a large conducting ground plane in the plane of measurement. The ground plane, consisting of a 1.3 meter by 1.3 meter foil covered piece of insulating foam, can be seen in placed in the bracket block in Figure 4.2. The center of the ground plane was located bore sight to the horn antennas. This is again a measurement that does not contain the desired tag response, but is needed for the data processing to obtain a pure isolated tag response. Ideally, the ground plane acts as an

"infinite" ground plane, allowing a pure observation of the horns' contributions to the measurement. In theory, this would be analogous to having a link with the horns pointed directly at each other. The expected observed responses contained in the ground plane measurement are found in Equation 4.2.

$$s_{12b} = Coupling(H_1, H_2) + G_1 G_2 (\frac{\lambda}{4\pi \times 2r})^2$$ **Equation 4.2**

In Equation 4.2, the contributions of the horns are accounted for by the terms G_1 and G_2. These terms will be referred to as "gain" terms as they include gain due to the antennas. However, they include all contributions to the measurement by the horns and could be considered as the transfer function of the antenna link rather than just simple gain terms. The remaining part of the term which includes G_1 and G_2 is simply to account for free space propagation to and from the large conducting ground plane. The coupling between the horns is again present and should take the same early time form as that in the reference measurement.

Figure 4.2-Ground Plane Measurement

The intent of this measurement is to capture the response of the horns so it can later be deconvolved from the response of the tag. The coupling measurement is again extraneous and of no use.

4.2.3 Tag Response Measurement

The final measurement is with the tag present. The measurement setup is pictured in Figure 4.3, and the tag can be seen placed in the bracket block using a strip of rigid foam. The tag was located bore sight to the antennas.

This is the measurement that contains the response of the tag which we want to isolate. The tag response is represented by the T term in Equation 4.3. The response of the horns, the response due to coupling between the horns, and background scattering are also present.

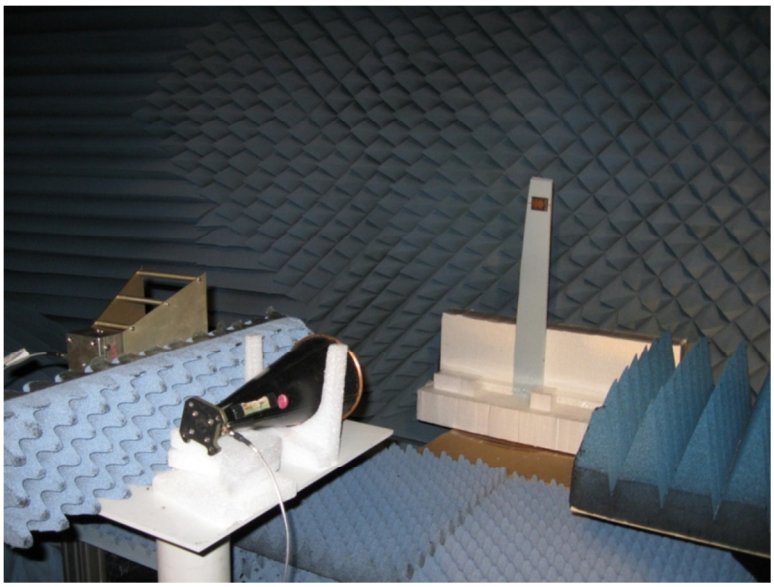

Figure 4.3-Measurement with tag present

$$s_{12c} = Coupling(H_1, H_2) + G_1 G_2 (\frac{\lambda}{4\pi \times 2r})^2 T + Background\ Scattering$$

Equation 4.3

It is worth noting that removal of background scattering, and the coupling between the horns could be mostly removed by windowing in the time domain as they are predominantly present as late time and early time responses respectively. We chose to proceed with the extra reference measurements and additional processing as a validation

of our measurement and analysis techniques. In the next section, we elaborate the data processing steps needed to isolate the tag response from our measurements.

4.3 Data Processing

In this section, the results of each step in the processes of isolating the tag response from the measured data will be considered. Only the case of the normally oriented co-polarized tag will be presented in detail. The results of each step in the data processing for the other tag orientations do not differ enough to warrant a comprehensive presentation.

4.3.1 Subtract Reference

The first step in processing the data in order to isolate the response of the tag is to remove the coupling between the horns and background scattering. This is accomplished via a subtraction operation in the frequency domain. The reference measurement is subtracted from the measurement with the tag present. The results of this subtraction can be seen in the time-domain. In Figure 4.4, the early time response attributable to the coupling and also the background scattering are removed as desired. It is not possible to separate which portion of the removed response was due to the coupling and which portion was due to background scattering. However, it probably safe to assume the coupling was larger in magnitude than background scattering, and thus the portion at 10 ns that was removed was due to the coupling.

The portion of the measurement corresponding to the scattering of the tag can now be seen starting at approximately 15 ns. Figure 4.5 shows an enlarged plot of the tag's response after subtracting the reference. As expected, the response takes the semblance of a summation of damped sinusoids. While the time-domain response of Figure 4.5 does contain the response of the tag, the contribution of the two horn antennas is still present. Further processing is required to completely isolate the tag's response.

$$s_{12d} = s_{12c} - s_{12a} = G_1 G_2 (\frac{\lambda}{4\pi \times 2r})^2 \mathrm{T} \qquad \textbf{Equation 4.4}$$

A time window was also applied to the subtracted waveform to remove any early and late time responses not completely removed by the subtraction operation. The tag response is causal and of limited duration. Anything before the onset of excitation at 15 ns cannot be due to the tag, and anything substantial remaining after the tag response has decayed cannot be due to the tag either. The 6.17 GHz pole was the lowest damped pole of our simulated ideal case pole signature. Based on its damping factor of -3.24E8, after 14.2 ns it has decayed to 1% of its initial value. Using 15 ns as a start time, and 29.2 ns as an end time, a window was applied as shown in Figure 4.6. The expected result of this windowing is that the frequency domain form of the tag's response will be cleaned up.

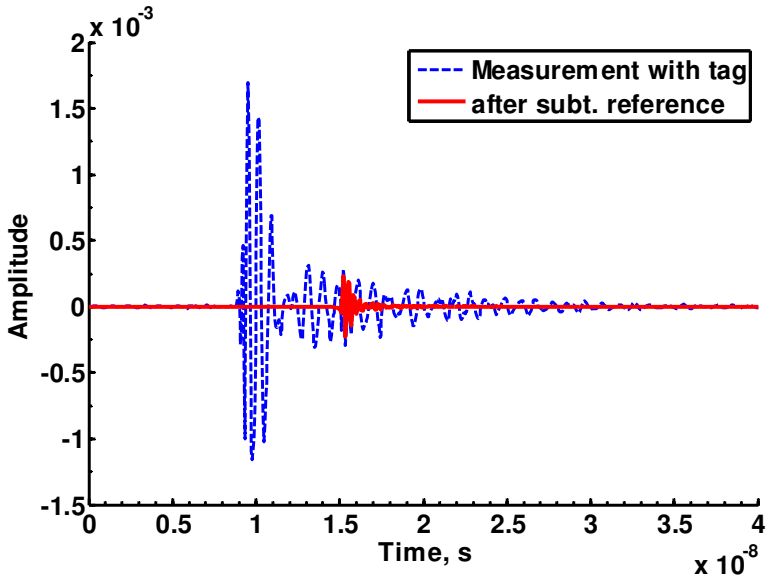

Figure 4.4-Tag Measurement before and after subtracting the reference measurement.

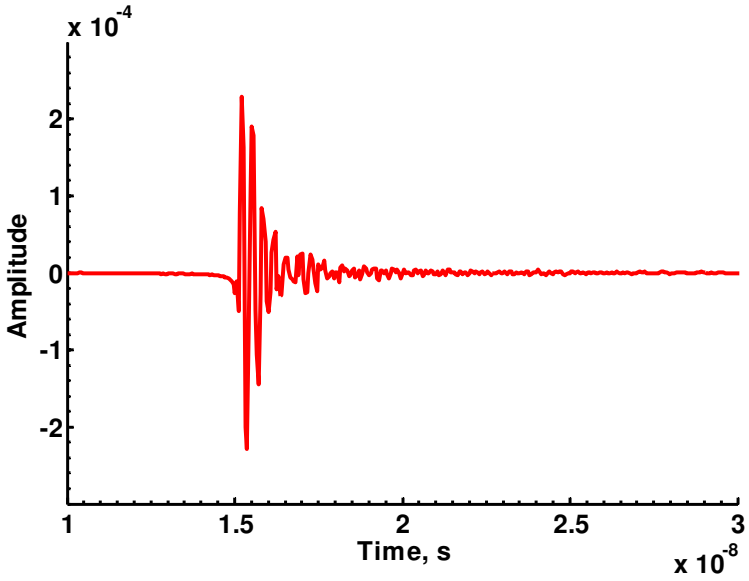

Figure 4.5-Enlarged portion of the tag measurement after subtracting the reference measurement.

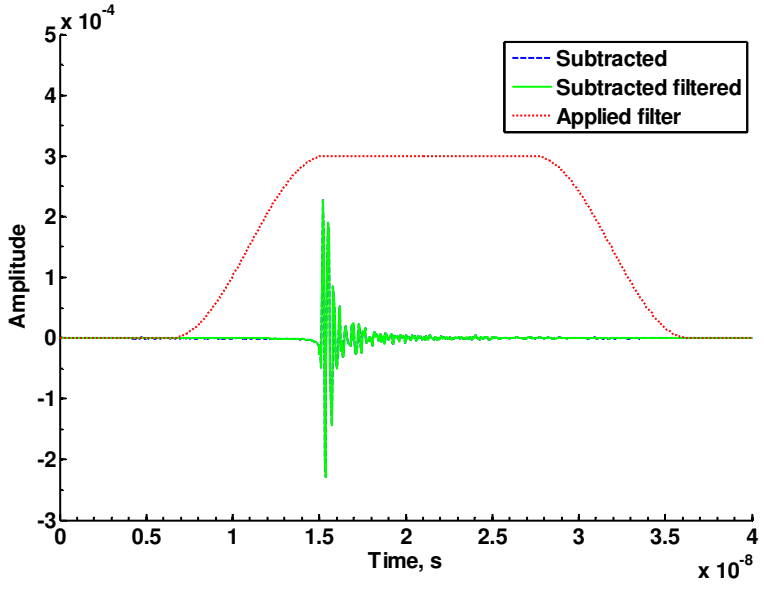

Figure 4.6-Windowing applied to the subtracted tag measurement

4.3.2 Remove Horn Response

To remove the response of the horns from the response of the tag we need to have a measurement containing only the response of the horns. The ground plane measurement

contains the desired response of the horns, but also coupling between the horns and background scattering. Removing these unwanted elements via a subtraction of the reference is not valid as it would be subtracting responses that due to the ground-plane are not present, instead effectively adding them.

To remove the coupling between the horns and background scattering from the ground-plane measurement we take the measurement to the time domain, and employ a time window as shown in Figure 4.7. The early time responses and late time responses are windowed out, and the response of the horns at 15 ns is retained. This process is represented by the second line of Equation 4.5.

$$
\begin{aligned}
& s_{12b} \xrightarrow{Inverse\ Fourier\ Transform} S_{12b}(t) = f_c(t) + f_{hgh}(t) \\
& \xrightarrow{Time\ Gaiting} S_{12b}^{tg}(t) = f_{hgh}(t) \\
& \xrightarrow{Fourier\ Transform} s_{12b}^{tg} = G_1 G_2 \left(\frac{\lambda}{4\pi \times 2r} \right)^2
\end{aligned}
$$

Equation 4.5

We now have a horn response measurement that is for the most part free of coupling and or background scattering. The windowed time domain ground plane measurement is taken back to the frequency domain, and the resulting isolated horn response is represented in right hand term of the last line of Equation 4.5.

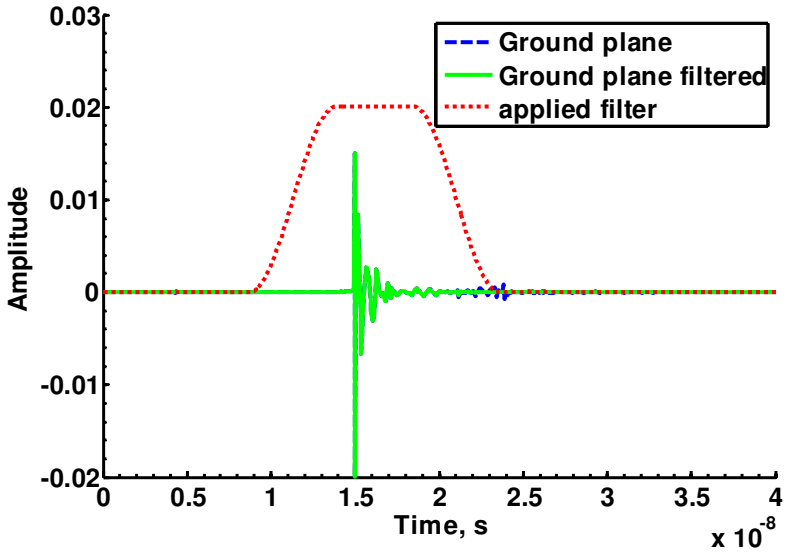

Figure 4.7-Measurement taken with ground plane present. The time windowing used to remove unwanted signals is indicated

4.3.3 Isolated Tag Response

The final step of isolating the tag response is accomplished in the frequency domain. The horn response is deconvolved from the tag response via a division of the subtracted windowed tag measurement by the windowed ground-plane measurement. This operation is shown in Equation 4.6, and the result is T, the transfer function representing the impulse response of the tag.

$$\frac{S_{12\mathrm{d}}}{S_{12b}^{tg}} = \mathrm{T} \qquad \textbf{Equation 4.6}$$

The next section considers the isolated response pole signature. First we will consider the effects of isolating the tag response in the frequency domain. The process of subtraction, windowing, and deconvolution has had several effects upon the data. In theory, the tag and the ground plane were located the same distance from the horns, and so they should have the same time delay. This time delay is represented by a linear phase progression in the frequency domain. Deconvolving the horn response from the subtracted tag response measurement should remove this phase progression, and the

corresponding time delay. The onset of the time domain tag response should now be at 0 s. Looking at the fully processed response in Figure 4.8, it does in fact appear that the response was moved to an onset of ~0 s. While the removal of the time delay worked well in this case, such is not always true. It was sometimes found necessary to add back in a time delay to ensure continuity of the waveform. The amount of delay added was done by inspection and trial and error. The waveform ultimately used for a pole extraction for the ideal measured case had some time delay added and is shown in Figure 4.9.

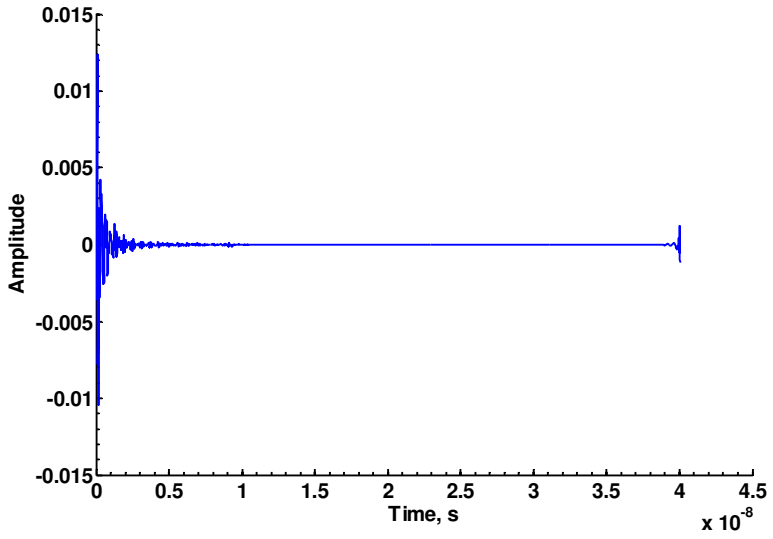

Figure 4.8- Time domain scattered response of the measured ideal case after fully processing the measured results.

The convolution also has the effect of bringing out an issue that was anticipated. For frequencies below 3 GHz, in the frequency domain response we can see the behavior of the horns becoming unstable. This limitation was acknowledged and anticipated. To correct for this, the data below 3 GHz was replaced assuming a magnitude relationship to frequency of f^4, and extrapolating the phase based on an assumed linear phase response for the data. The magnitude relationship was chosen based on assuming Rayleigh scattering behavior.

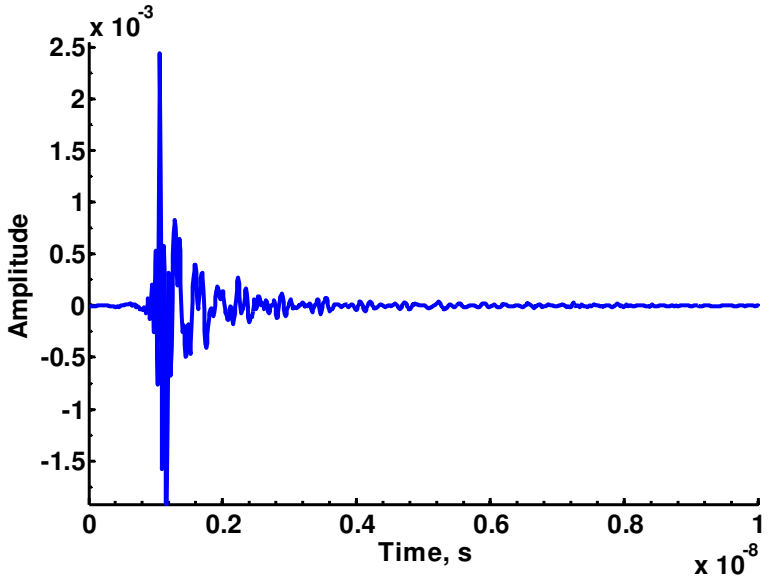

Figure 4.9-Time domain scattered response of the measured ideal case after fully processing the measured results with an added time shift.

Deconvolving the horn response also has the effect of normalizing the measured results, ultimately bringing results up in magnitude. The normalizing effect includes removing the gain of the horns, normalizing the excitation, removing losses in the system, and also removing free space path loss. This brings us to a form that can be directly compared to the simulations that is directly related to the RCS (for an analysis of this see Appendix A). The quantities represented are power in dB referenced to the incident power, and as can be seen in Figure 4.11 the simulations and measurements are at a similar level. The reason they are not exactly the same level is discussed in Appendix A as well.

The windowing of the subtracted tag response has had the cleaning effect that was predicted. The final form after all processing including the time-windowing of the subtracted tag response is represented by the dashed blue plot in Figure 4.10. Comparing this to the solid red plot, which represents a subtracted and deconvolved response, shows the windowing has had the effect of cleaning up the response. Whether or not this is beneficial for our goal of extracting poles was not determined.

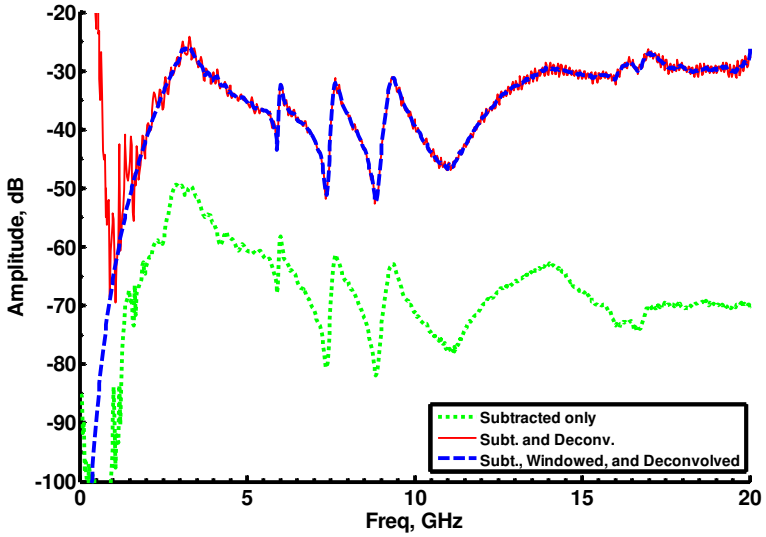

Figure 4.10-Measured frequency domain scattering response of the ideal case for various points in the data processing.

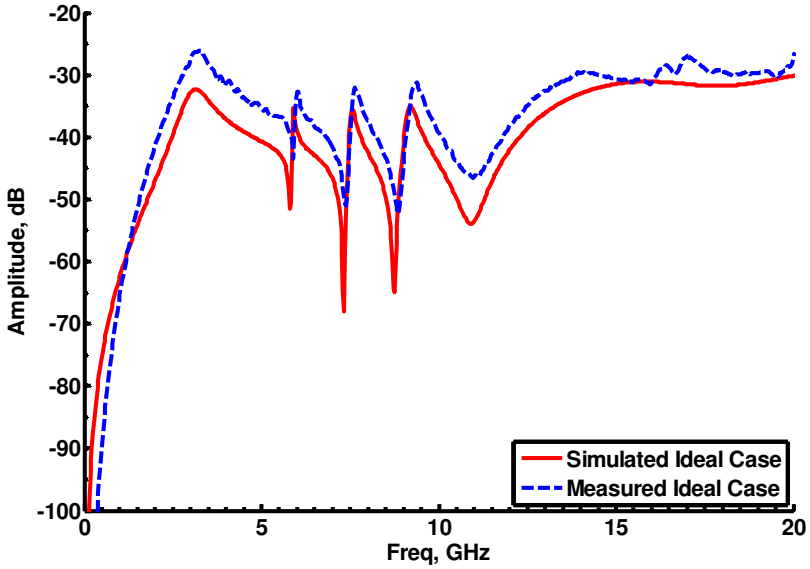

Figure 4.11-Comparison of the simulated and fully processed measured results for the ideal case.

4.4 Extracting Poles

4.4.1 Time Windowing

Once the data measured data has been fully processed, we can proceed to considering a singularity based analysis. The matrix pencil algorithm operates in the time domain, and we take our measured to the time domain via an IFFT. The resulting time domain waveform is the measured scattering response of the tag to an impulsive plane wave excitation. The same considerations exist for measurements as the simulations. Again, because our data is of limited bandwidth, the excitation is not an ideal impulse. This is of particular importance because if we consider parts of the waveform that contain the excitation, we are not necessarily extracting the poles corresponding to the natural response of the tag. To ensure that we are considering the source free response of the tag, we must use a time window that considers the late time and is free of the excitation.

The time window used to extract the poles is indicated by the red box in Figure 4.12. Unlike the simulations, there was not an exact start time that could be determined. In theory, the deconvolution operation should have moved the start time of any response to 0 s. However, as noted previously the deconvolution was imperfect about removing the linear phase term accounting for the time delay, and in some cases it was found necessary to artificially add a delay. The minimum start time was determined by inspection for each case. The peak of the response should indicate the peak of excitation. Looking at the time domain response, the peak occurs at 1.1 ns. Using this as a starting point and after some experimentation with subsequently later starting time windows, a time window starting at 1.6 ns was found suitable. Recall that for the simulations we were able to use the same start time for all simulations. This is not feasible for measurements due to the possibility of variation. Therefore, it was found necessary to repeat the process of determining a time window start time via inspection and experimentation for each measurement.

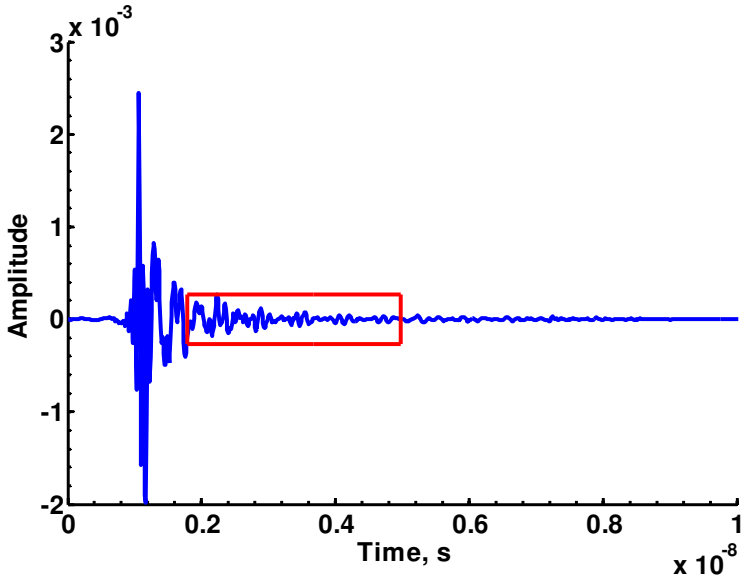

Figure 4.12-Time window used for the pole extraction from the fully processed measured ideal case tag response.

4.4.2 Measured Pole Signature. Have we successfully read the tag?

If we take our selected section of the isolated tag response, and apply the Matrix pencil algorithm, we extract the poles of Figure 4.13. Initially multiple poles were extracted where we would expect a single pole based on the simulations. Using the SVD sorting parameter by gradually reducing it, the groups are reducible to a single pole. We will consider the signature extracted for an SVD sorting parameter of $p = 2$ represented by the circles as our extracted signature. Comparing the extracted signature shows that we do in fact have a measured pole signature that by inspection matches the simulated pole signature. We have achieved the main goal of this thesis. The tag has been successfully read!

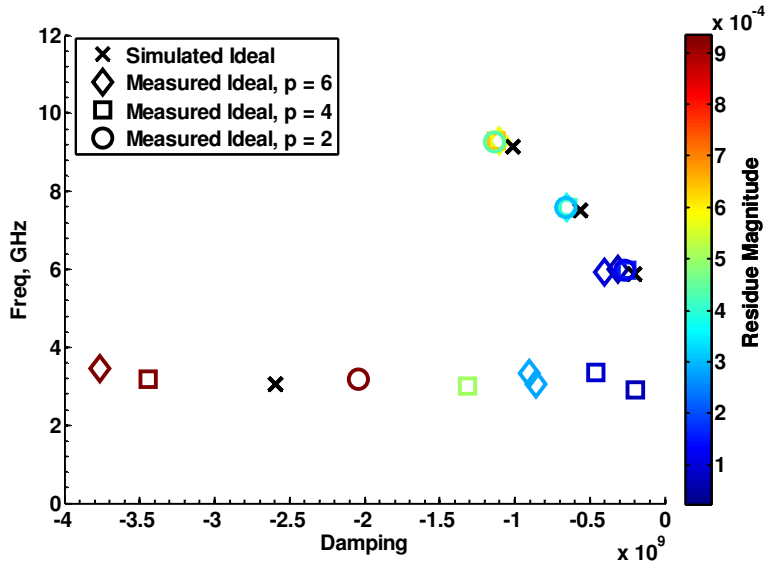

Figure 4.13-Pole Signature from measurements of the ideal case with different SVD sorting thresholds indicated by p.

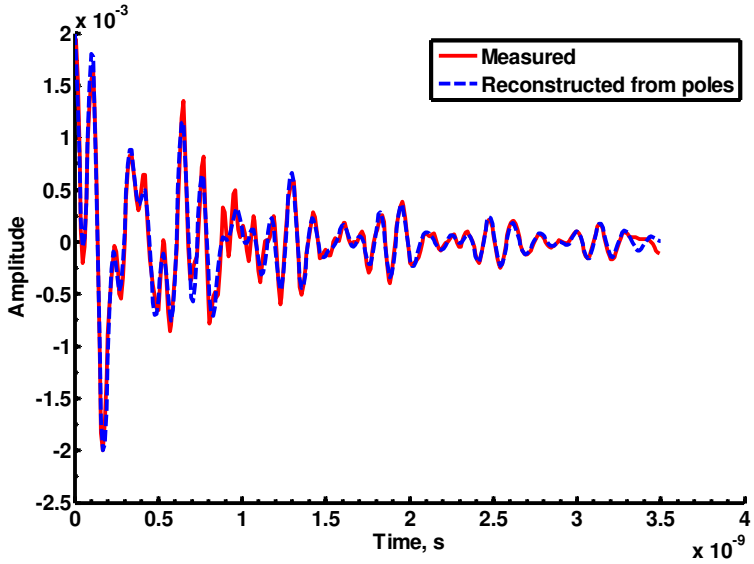

Figure 4.14-Comparison of the time domain response reconstructed from extracted poles v. the original.

4.4.3 Measured Edge Co-Polarized

After having successfully read the tag for the measured ideal orientation, we now turn our attention to an alternative case. For the tag to be of any practical use, it must be

readable for non-ideal situations. To this end we will consider the extreme case of having the tag completely on edge and co-polarized. In terms of our co-ordinate system in Figure 3.3, this is $\theta_{exc} = \theta_{obs} = 0°$, $\varphi_{exc} = \varphi_{obs} = 0°$, $\eta = 90°$, and $r = 1\ m$.

It becomes immediately evident based on the frequency domain response of Figure 4.15 that the measurements with the same data processing steps as used for the measured ideal case closely resembles. This is very promising for a successful pole signature read.

Using a SVD sorting parameter of $p = 2$, the resulting extracted poles in Figure 4.16 do in fact resemble the simulated case as well as the ideal case signature. Again, we have successfully read the tag, but this time for a drastically different orientation.

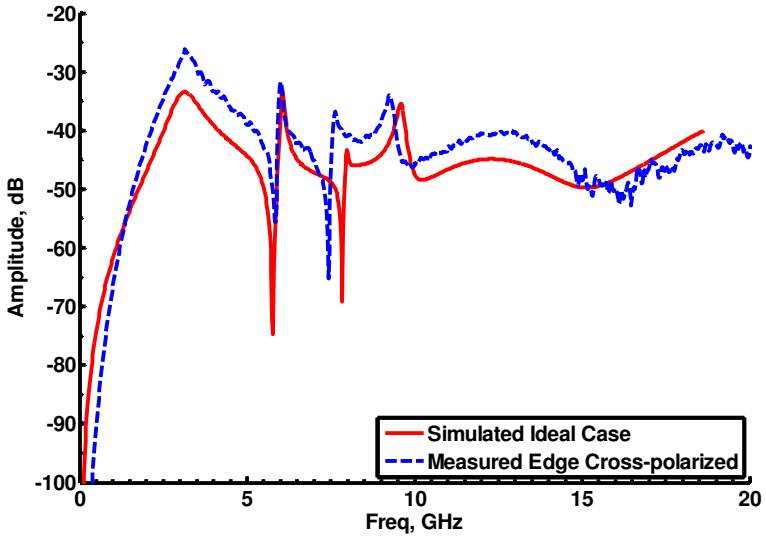

Figure 4.15-Measured Frequency Domain scattering response of the notched elliptical dipole tag with the tag on edge and co-polarized.

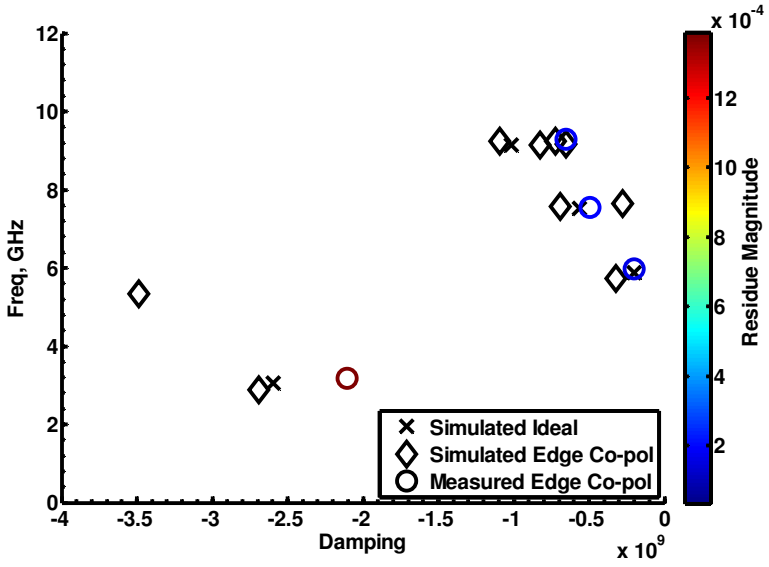

Figure 4.16-Pole Signature from measurements of the on edge co-polarized case.

4.4.4 Measured Edge Cross-Polarized

Based on our simulation results, it was predicted that for the case of having the tag on edge and with cross-polarized excitation we would not be able to observe the poles. This is in fact the case. Despite varying the time-window and altering the sorting parameter, a pole-signature matching that of our simulations was not extracted.

Even with not being able to extract the pole, the frequency domain form of the measured scattered fields as shown in Figure 4.17 should still resemble the simulations. For the other two measurements presented, the resulting fully processed frequency domain response differed from the simulated response by about 5 dB in magnitude, whereas the measurements for this case differ by 40 dB or more. It is possible an error occurred while taking the measurement

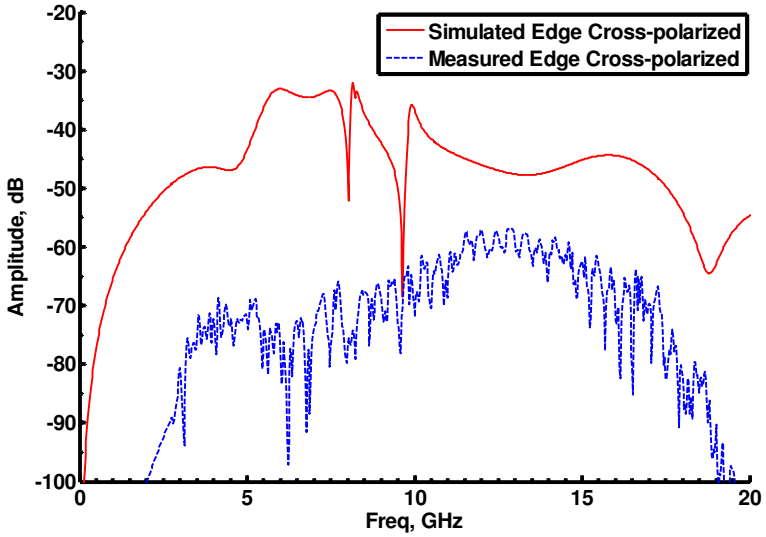

Figure 4.17-Frequency domain scattered response of the notched elliptical pole tag on edge and cross-polarized.

4.5 Conclusions

In this chapter, the ultimate goal of this thesis, to successfully read a chipless RFID tag using a singularity based signature, was achieved. The tag was measured using a monostatic radar type setup, and after some data processing, a pole signature matching that obtained in Chapter 3 was extracted. The tag was successfully read for a normal and on-edge orientation when co-polarized. The tag was found not readable when cross-polarized.

CHAPTER 5

Conclusions

This thesis achieved its ultimate goal of successfully reading a real embedded singularity tag. This chapter briefly summarizes the work leading up to this point, and suggests several topics for future work that arose through the course of this thesis.

5.1 Summary of work presented

We were able to take an existing chipless RFID tag with observable intentionally created features, specifically nulls, in the frequency domain scattering behavior, and extract a pole singularity representation of the scattered electric field. Each pole was experimentally verified to be attributable to corresponding physical features of the tag structure specifically the base dipole structure and the notches. The resulting poles from the simulation results were used to define pole signatures. Next, a prototype tag was measured. Three tag orientations were consider; the ideal case of a normally oriented co-polarized tag, the on edge co-polarized case, and the on edge cross-polarized case. After data processing to isolate the tag's scattered response, a pole signature was extracted from the measurements. For the two co-polarized case the measured pole signature was

fond to match the simulated, indicating that the tag was successfully read. The tag was found to be readable even when on edge, but only when co-polarized.

5.2 Future Work

The following are topics that may be worth considering to expand the research in this thesis

1. Develop an application specific pole extraction algorithm, which could consist of a modified Matrix pencil algorithm.
2. Analyze the effects of using the SVD sorting parameter. The SVD sorting feature was used to achieve an end, but the meaning of the sorting process was not analyzed. What was thrown out, and did it have any useful properties?
3. Determine an exact mechanism for creating/manipulating poles. It was noted that poles do not result simply from the nulls, though they do appear to contribute towards the creation of the pole singularities. The narrowband versus wideband observations regarding damping also fall into this topic. The creation of poles is not limited to notches, and other structures could be of interest.
4. Determine a reference pole signature based on more comprehensive simulations involving variations in aspect. The ideal orientation pole signature was used a reference signature. While the simulated ideal case reference signature served its purpose in the thesis, it became apparent that other poles existed when variations in aspect were introduced. These poles, while seemingly a complication, may be beneficial for the purposes of extracting the data.
5. Increase the data capacity. 3 bits is of limited practicality. How many singularities can be embedded?
6. Investigate the extra utility of the pole and residue parameters. Poles were the parameter of interest (frequency and damping), however the information contained in the residues (phase, magnitude) could also be useful not only for the purposes of encoding data, but also for the purposes of remote sensing.

7. Develop a tag reading algorithm. It was an acknowledged limitation throughout the thesis that the interpretation of results relied completely on visual inspection. Having a reading algorithm would allow for some quantifiable assertions to be made.
8. Measure tags with different bit sequences encoded. Simulations were only considered for the permutations. Actual measurements of real tag permutations would certainly be of interest.
9. Develop a tag reader. In reality, these suggestions for future work when combined suggest a single goal; construct a reader. The majority of the listed suggestions for future work are not mutually exclusive. An endeavor that seeks to construct an autonomous reader might be the best course of action with each individual suggestion being a piece of this process.

REFERENCES

[1] D. D. Mawhinney, "Microwave Tag Identification Systems," *Rca Review,* vol. 44, pp. 589-610, 1983.

[2] K. V. S. Rao, "An overview of backscattered radio frequency identification system (RFID)," in *Microwave Conference, 1999 Asia Pacific*, 1999, pp. 746-749 vol.3.

[3] L. Reindl*, et al.*, "SAW devices as wireless passive sensors," in *Ultrasonics Symposium, 1996. Proceedings., 1996 IEEE*, 1996, pp. 363-367 vol.1.

[4] L. Reindl and W. Ruile, "Programmable reflectors for SAW-ID-tags," in *Ultrasonics Symposium, 1993. Proceedings., IEEE 1993*, 1993, pp. 125-130 vol.1.

[5] A. Blischak and M. Manteghi, "Pole-Residue Analysis of a Notched UWB Elliptical Dipole Tag," presented at the URSI-USNC National Radio Science Meeting, Boulder, CO, 2009.

[6] A. Blischak and M. Manteghi, "Pole Residue Techniques for Chipless RFID Detection," presented at the IEEE Antennas & Propagation Symposium, Charleston, SC, 2009.

[7] M. Brandl*, et al.*, "A new anti-collision method for SAW tags using linear block codes," in *Frequency Control Symposium, 2008 IEEE International*, 2008, pp. 284-289.

[8] S. Preradovic*, et al.*, "Chipless Frequency Signature Based RFID Transponders," in *Microwave Conference, 2008. EuMC 2008. 38th European*, 2008, pp. 1723-1726.

[9] S. Preradovic and N. C. Karmakar, "Design of fully printable planar chipless RFID transponder with 35-bit data capacity," in *Microwave Conference, 2009. EuMC 2009. European*, 2009, pp. 013-016.

[10] M. Manteghi and Y. Rahmat-Samii, "Frequency notched UWB elliptical dipole tag with multi-bit data scattering properties," in *Antennas and Propagation Society International Symposium, 2007 IEEE*, 2007, pp. 789-792.

[11] Z. Lu*, et al.*, "An innovative fully printable RFID technology based on high speed time-domain reflections," in *High Density Microsystem Design and Packaging*

and Component Failure Analysis, 2006. HDP'06. Conference on, 2006, pp. 166-170.

[12] L. B. Felsen and C. E. Baum, *Transient electromagnetic fields*. Berlin ; New York: Springer-Verlag, 1976.

[13] C. Baum, "The singularity expansion method: Background and developments," *Antennas and Propagation Society Newsletter, IEEE,* vol. 28, pp. 14-23, 1986.

[14] C. E. Baum*, et al.*, "The singularity expansion method and its application to target identification," *Proceedings of the IEEE,* vol. 79, pp. 1481-1492, 1991.

[15] C. E. Baum, "On the Singularity Expansion Method for the Solution of Electromagnetic Interaction Problems," *Interaction Notes,* vol. EMP-3, pp. 1-111, 1971.

[16] C. E. Baum, "Direct construction of a ξ-pulse from natural frequencies and evaluation of the late-time residuals," in *Ultra-Wideband Short-Pulse Electromagnetics 4, 1998*, 1998, pp. 349-360.

[17] M. VanBlaricum and R. Mittra, "Problems and solutions associated with Prony's method for processing transient data," *Antennas and Propagation, IEEE Transactions on,* vol. 26, pp. 174-182, 1978.

[18] Y. Hua and T. K. Sarkar, "Matrix pencil method for estimating parameters of exponentially damped/undamped sinusoids in noise," *Acoustics, Speech and Signal Processing, IEEE Transactions on,* vol. 38, pp. 814-824, 1990.

[19] Y. Hua and T. K. Sarkar, "On SVD for estimating generalized eigenvalues of singular matrix pencil in noise," *Signal Processing, IEEE Transactions on,* vol. 39, pp. 892-900, 1991.

[20] S. Licul. (2004). *Ultra-wideband antenna characterization and modeling*. Available: http://scholar.lib.vt.edu/theses/available/etd-11072004-200046/

[21] H. G. Schantz*, et al.*, "Frequency notched UWB antennas," in *Ultra Wideband Systems and Technologies, 2003 IEEE Conference on*, 2003, pp. 214-218.

APPENDIX A

Quantities represented by the simulations and measurements

Measurements

If we apply the radar equation to the tag measurement we get

$$P_{rx}^{tag} = \frac{P_{tx}G_{tx}G_{rx}\lambda^2\sigma_{tag}}{(4\pi)^3 r^4}$$

For the ground plane measurement, we will assume image theory applies, and use the Friis equation with the link distance equaling twice the observation distance.

$$P_{rx}^{ref} = P_{tx}G_{tx}G_{rx}\left(\frac{\lambda}{4\pi d}\right)^2$$

Where $d = 2r$

$$P_{rx}^{ref} = P_{tx}G_{tx}G_{rx}\left(\frac{\lambda}{4\pi 2r}\right)^2 = \frac{P_{tx}G_{tx}G_{rx}\lambda^2}{(4\pi)^2 4r^2}$$

The normalizing effect of the deconvolution operation is represented as

$$\frac{P_{rx}^{tag}}{P_{rx}^{ref}} = \frac{P_{tx}G_{tx}G_{rx}\left(\frac{\lambda}{4\pi d}\right)^2}{\frac{P_{tx}G_{tx}G_{rx}\lambda^2}{(4\pi)^2 4r^2}} = \frac{\frac{\cancel{P_{tx}}\cancel{G_{tx}}\cancel{G_{rx}}\cancel{\lambda^2}\sigma_{tag}}{(4\pi)^3 r^4}}{\frac{\cancel{P_{tx}}\cancel{G_{tx}}\cancel{G_{rx}}\cancel{\lambda^2}}{(4\pi)^2 4r^2}} = \frac{\sigma_{tag}}{4\pi r^2}$$

Simulations

One definition for radar cross section is

$$\sigma = 4\pi r^2 \frac{S_r}{S_i} = 4\pi r^2 \frac{|E_s|^2/\eta_0}{|E_i|^2/\eta_0} = 4\pi r^2 \frac{|E_s|^2}{|E_i|^2}$$

If we apply this to the simulation results which consider the scattered electric fields at a point in space

In the simulations, $E_i = 1\frac{V}{m}$, thus

$$\sigma = 4\pi r^2 \frac{|E_s|^2}{1\frac{V^2}{m^2}}$$

If we manipulate to get to a form considered in the plots

$$\frac{|E_s|^2}{1\frac{V^2}{m^2}} = \frac{\sigma}{4\pi r^2}$$

These are the quantities considered for both the measurements and simulations. It is equivalent to scattered power normalized to incident power.